Clinical Science (2021) **135** 829–846
https://doi.org/10.1042/CS20201496

PORTLAND PRESS

Research Article

SOX7 suppresses endothelial-to-mesenchymal transitions by enhancing VE-cadherin expression during outflow tract development

Xuechao Jiang[1,*], Tingting Li[2,*], Bojian Li[2], Wei Wei[2], Fen Li[3], Sun Chen[2], Rang Xu[1] and Kun Sun[2]

[1]Scientific Research Center, Xinhua Hospital, Affiliated to Shanghai Jiao Tong University School of Medicine, Shanghai 200092, China; [2]Department of Pediatric Cardiology, Xinhua Hospital, Affiliated to Shanghai Jiao Tong University School of Medicine, Shanghai 200092, China; [3]Department of Pediatric Cardiology, Shanghai Children's Medical Center, Affiliated to Shanghai Jiao Tong University School of Medicine, Shanghai 200127, China

Correspondence: Rang Xu (182306@shsmu.edu.cn) or Kun Sun (sunkun@xinhuamed.com.cn)

The endothelial-to-mesenchymal transition (EndMT) is a critical process that occurs during the development of the outflow tract (OFT). Malformations of the OFT can lead to the occurrence of conotruncal defect (CTD). *SOX7* duplication has been reported in patients with congenital CTD, but its specific role in OFT development remains poorly understood. To decipher this, histological analysis showed that SRY-related HMG-box 7 (SOX7) was regionally expressed in the endocardial endothelial cells and in the mesenchymal cells of the OFT, where EndMT occurs. Experiments, using *in vitro* collagen gel culture system, revealed that SOX7 was a negative regulator of EndMT that inhibited endocardial cell (EC) migration and resulted in decreased number of mesenchymal cells. Forced expression of SOX7 in endothelial cells blocked further migration and improved the expression of the adhesion protein vascular endothelial (VE)-cadherin (VE-cadherin). Moreover, a *VE-cadherin* knockdown could partly reverse the SOX7-mediated repression of cell migration. Luciferase and electrophoretic mobility shift assay (EMSA) demonstrated that SOX7 up-regulated VE-cadherin by directly binding to the gene's promoter in endothelial cells. The coding exons and splicing regions of the *SOX7* gene were also scanned in the 536 sporadic CTD patients and in 300 unaffected controls, which revealed four heterozygous *SOX7* mutations. Luciferase assays revealed that two *SOX7* variants weakened the transactivation of the *VE-cadherin* promoter. In conclusion, SOX7 inhibited EndMT during OFT development by directly up-regulating the endothelial-specific adhesion molecule VE-cadherin. *SOX7* mutations can lead to impaired EndMT by regulating VE-cadherin, which may give rise to the molecular mechanisms associated with SOX7 in CTD pathogenesis.

Introduction

Congenital heart defect (CHD) is the most common form of human birth defects, affecting nearly 1 in 100 live births [1,2]. Within the scope of CHD, conotruncal defect (CTD) including Tetralogy of Fallot (TOF), double outlet right ventricle (DORV), transposition of the great arteries (TGA), pulmonary atresia (PA), and persistent truncus arteriosus (PTA), account for 30% of human CHD, which causes significant morbidity and mortality [3]. CTD is also known as outflow tract (OFT) defect. The cardiac OFT is a temporary cylindrical structure positioned at the heart's arterial pole and connects the aortic sac and aortic arch arteries to the ventricles. The OFT is formed through interactions between multiple cardiac lineages, such as endocardial cells (ECs) and cardiomyocytes located within the heart itself, in addition to the migrating cells arising from the cardiac neural crest (CNC) [2]. A subpopulation of ECs undergo endothelial-to-mesenchymal transition (EndMT) and migrate into the cardiac jelly, and together,

[*]These authors contributed equally to this work.

Received: 17 December 2020
Revised: 06 March 2021
Accepted: 15 March 2021

Accepted Manuscript online: 15 March 2021
Version of Record published: 26 March 2021

Clinical Science (2021) **135** 829–846
https://doi.org/10.1042/CS20201496

with the CNC cells, give rise to the OFT cushions [4–8]. Multiple critical genes and signaling pathways are involved in cardiac OFT development, including Tbx1 and Hand factors, with signaling occurring through the fibroblast growth factor, bone morphogenetic protein (BMP), and Notch [2,3]. However, because of the complex nature of CTD, the etiology of most cases remain poorly understood. Identifying CTD-causing genes and its underlying molecular mechanisms are required to gain a greater understanding of CTD development.

We previously reported the identification of a *SOX7* duplication in a pediatric patient in a family with congenital CTD, which was further verified in sporadic cases of CTD [9]. It was the first published evidence that *SOX7* was strongly associated with CTD [9]; however, the molecular mechanisms of this association remain to be explored. *SOX7*, as a member of the SOX (SRY-related HMG-box) family of transcription factors, has been widely studied in vasculogenesis [10–12], hematopoiesis [13–15] development, and tumorigenesis [16–18].

There is also intriguing evidence that suggests that SOX7 is necessary for cardiogenesis. SOX7 is expressed in the mouse and human heart [19,20], and is also found in the early cardiogenic region of *Xenopus* embryos [21]. Interestingly, combined morpholino knockdown of *sox7* and *sox18* promotes severe vascular and cardiac defects in both zebrafish and *Xenopus* embryos [10,21–23]. *Sox7*-knockout mice exhibit signs of delayed development, dilated pericardial sacs, and failure of yolk sac remodeling by E10.5, which are suggestive of cardiovascular failure [24]. The molecular and pathogenic mechanisms of SOX7 in heart development—especially cardiac OFT defects—are far from clarified.

In the present study, we demonstrate that SOX7 is expressed in the endocardial endothelial and mesenchymal cells, where EndMT occurs during OFT development. We performed OFT explant assays and cell function analyses that indicated that SOX7 acts as a negative regulator of EC migration during EndMT. SOX7 exerts its function as a negative regulator by increasing the transcription of vascular endothelial (VE)-cadherin (VE-cadherin) by directly binding to its promoter. We scanned the coding exons and splicing regions of the *SOX7* gene and identified four heterozygous *SOX7* mutations in 536 patients with CTD. Luciferase assays revealed that two variants had decreased their transcriptional activity when associating with the *VE-cadherin* promoter, this likely occurs due to a reduced protein expression or altered DNA-binding to VE-cadherin. These results provide novel insight into the molecular mechanisms associated with *SOX7* in CTD pathogenesis.

Materials and methods

Mice

C57BL/6 mice were acquired from the Shanghai SLAC Laboratory Animal Co., Ltd. (Shanghai, China), which were bred in the animal facility of Xinhua Hospital under specific pathogen-free (SPF) barrier conditions. Mouse embryos generated from timed C57BL/6 matings were staged according to the number of tail somites present. Stage 10.5, 11.5, and 12.5 days post coitus (dpc) embryos were used for histological analysis and explant assay. Euthanasia was performed by CO_2 gas in a closed chamber followed by cervical dislocation, embryos were isolated and processed following standard procedures.

All animal procedures conformed to the Guidelines for the Care and Use of Laboratory Animals published by the National Institution of Health and was approved by the Institutional Animal Care and Use Committee (IACUC) of the Shanghai Jiao Tong University School of medicine. All animal experiments were performed at the Xinhua hospital.

Human samples

The pregnant women who could not continue pregnancy for certain reasons, and elective medical termination of pregnancy were performed at Department of Obstetrics and Gynecology of Xinhua Hospital during the first trimester under the Maternity Protection Law of China. All human embryonic samples were obtained voluntarily after the donors signed the informed consents from Xinhua Hospital, Affiliated to Shanghai Jiao Tong University School of Medicine. The present study was approved by the Medical Ethics Committee of Xinhua Hospital (no. XHEC-C-2012-018). After the aborted embryos were transported to the laboratory, they were isolated with an Olympus stereomicroscope and categorized in accordance with the Carnegie stage (CS). The well-preserved specimens evaluated as normal, were fixed in 4% paraformaldehyde (PFA) overnight, embedded in paraffin sagitally, and then sectioned at the thickness of 4 μm.

DNA samples were obtained from peripheral venous blood of 536 sporadic patients with proven cardiac OFT defects, including 234 TOF, 98 PA/VSD, 13 PA/IVS, 92 TGA, 99 DORV (Table 1). Control DNA samples were obtained from 300 normal subjects. All the participants were recruited from Xinhua Hospital and Shanghai Children's Medical Center. Diagnosis of patients with cardiac OFT defects were confirmed by echocardiography, cardiac catheterizations examinations or other operation recordings. Patients with chromosomal abnormalities or syndromic cardiovascular

Table 1 Frequency and spectrum of CTD patients

Cardiac defects	Number	Percentage
TOF	234	43.66%
PA/VSD	98	18.28%
PA/IVS	13	2.43%
TGA	92	17.16%
DORV	99	18.47%
Total	536	100%

Abbreviations: PA/IVS, PA with intact ventricular septum; PA/VSD, PA with ventricular septal defect.

Table 2 Clinical information and mutations of *SOX7* in patients with CTD

Patient no.	Gender	Age	Cardiac pheno-type	Location	Nucleotide change	Amino acid change	Mutation taster	PolyPhen-2	SIFT	gnomAD	ExAC
F117	F	6 years	TOF/ASD	exon1	40C>G	L14V	Disease-causing	0.731	0.039	0.000006439	0.00001267
F200	F	3 months	TOF/PS	exon2	458G>A	R153Q	Disease-causing	0.547	0.69	0.000008208	
F126	M	1 year	TOF/PFO	exon2	515C>G	P172R	Disease-causing	0.992	0.005		
F192	M	13 years	TOF/PS	exon2	559G>A	G187S	Disease-causing	0.344	0.277	0.000004162	

Abbreviations: ASD, atrial septal defect; F, female; M, male; PFO, patent foramen ovale; PS, pulmonary stenosis.
The standard of each scoring software is: Mutation Taster gives a judgment of the risk of mutation, divided into 'disease-causing' and 'polymorphism'; PolyPhen-2 score < 0.5 (Benign), >0.5 (possibly damaging), the closer the score is to 1, the higher the risk of disease (probably damaging); SIFT software score ≤ 0.05 (harmful), >0.05 (harmless).

defects were excluded. The human experimentations were approved by the Medical Ethics Committee of Xinhua Hospital (no. XHEC-C-2012-018) and Shanghai Children's Medical Center (no. SCMC-201015). Fully written informed consent was obtained from all participants or their guardians, and all of them approved to publish the case details. All procedures were in accordance with the ethical standards of the institutional and national research committees and the Declaration of Helsinki.

Mutation screen

Mutation screen of the coding region and flanking intro-exon boundaries of *SOX7* were conducted by FastTarget™ technology (Genesky Biotechnologies Inc, Shanghai, China) [25]. Nonsynonymous mutations in the coding and splicing regions of *SOX7* with a prevalence of under 0.1% in control populations (under 0.1% in both the 300 healthy individuals and public variant databases, including ExAC and genomeAD). The candidate variants were validated by Sanger sequencing, and primers used in the present study are summarized in Supplementary Table S1. Pathogenicity of all the mutations were predicted by programs including Mutation Taster (http://www.mutationtaster.org/), Polyphen-2 (http://genetics.bwh.havard.edu/pph2/), SIFT (http://provean.jcvi.org/index.php) (Table 2).

Plasmids and mutagenesis

To generate the wild-type (WT) SOX7 expression plasmid, a full length of human SOX7 ORF was inserted into pcDNA3.1(+) vector. Using WT plasmids as the templates, four specific mutations were generated by the QuikChange XL site-directed mutagenesis kit (Stratagene, La Jolla, California, U.S.A.), and the site mutagenesis primers were summarized in Supplementary Table S1. To generate the *VE-cadherin* promoter luciferase reporter plasmid, the human *VE-cadherin* promoter segment −534/+45 bp (transcription start site as +1, primer in Supplementary Table S1) was inserted into pGL3-basic reporter vector, which was homologous to previously described *VE-cadherin* promoter in mouse [13]. The integrity of all plasmid inserts were verified by Sanger sequencing.

Clinical Science (2021) **135** 829–846
https://doi.org/10.1042/CS20201496

Cell culture and transfection assays

Human umbilical vein endothelial cell (HUVEC), human embryonic kidneys (HEK)-293T, C2C12 (mouse myoblasts), H9C2 (rat cardiac myoblasts) cells were obtained from Cell Bank of Chinese Academy of Sciences. After the cells were acquired, they were expanded for 3–5 passages and then divided into many independent aliquots and stored in liquid nitrogen. The independent aliquot of cells were thawed, and passaged for P3–P6 to perform each experiment. HEK-293T, C2C12, and 293T cells were cultured in DMEM high-glucose medium (HyClone, SH30243.01, Utah, U.S.A.) with 10% fetal bovine serum (Gibco, 10437-028, California, U.S.A.) and 1% streptomycin/penicillin (Gibco, 15140122) in 37°C, 5% CO_2 humidified incubator. For luciferase reporter assay, cells were transfected with the expression plasmid pcDNA3.1-SOX7 and *VE-cadherin* promoter reporter plasmids using transfection reagent FuGENE HD (Promega, Madison, Wisconsin, U.S.A.). 293T cells were also transfected with WT and mutant SOX7 plasmid for Western blot analysis.

HUVECs were grown in F12K medium (HyClone, SH30526.01, Utah, U.S.A.) with 10% fetal bovine serum (Gibco, 10437-028, California, U.S.A.), containing 0.1 mg/ml heparin (Sigma–Aldrich), 0.03 mg/ml endothelial cell growth supplement (Sigma–Aldrich) and 1% streptomycin/penicillin (Gibco, 15140122) in 37°C, 5% CO_2 humidified incubator. HUVECs were transfected with *VE-cadherin* siRNA (Si-VE-cad, sequence in Supplementary Table S1) or with scrambled sequence as a control siRNA (Si-Con, sequence in Supplementary Table S1), or infected with adenovirus-encoding GFP (AdV-GFP) or SOX7 (AdV-SOX7) for real time-PCR, Western blot, cell proliferation and viability assay, wound healing and transwell analysis.

Western blot analysis

Cells were collected and lysed by RIPA buffer (Beyotime Biotech Inc., Shanghai, China), mixed with SDS loading buffer, and denatured at 100°C for 10 min. Protein were loaded and separated on 10% SDS/PAGE gels, then transferred to nitrocellulose membranes. Membranes were blocked at room temperature in 5% skim milk for 2 h, then incubated overnight at 4°C with anti-SOX7 (1:500, Sigma–Aldrich, HPA009065, RRID: AB_1857390), anti-VE-cadherin (1:1000, Abcam, ab33168, RRID: AB_870662), and anti-glyceraldehyde 3-phosphate dehydrogenase (GAPDH, 1:10000, Sigma–Aldrich, G9545, RRID: AB_796208) antibodies. After the membranes were rinsed, they were incubated with horseradish peroxidase (HRP)-conjugated anti-rabbit secondary antibody (1:10000, Jackson, 111-035-003, RRID: AB_2313567) for 1 h. Detection was performed by an enhanced chemiluminescence Western blot detection system (Millipore, Billerica, MA, U.S.A.). The densitometric analysis of immunoblots was performed by ImageJ software.

Immunohistochemistry

Paraffin-embedded embryo sections underwent deparaffinization, hydration, and antigen repair with citrate buffer (Beyotime biotechnology, China). Then quenched endogenous peroxidase activity with 3% H_2O_2, blocked in 5% BSA, and incubated with rabbit polyclonal antibody against SOX7 (Sigma–Aldrich, HPA009065, RRID: AB_1857390) overnight at 4°C. Next, the secondary antibody, HRP-labeled anti-rabbit immunoglobulin (Gene Tech, Shanghai, China) was applied for 45 min at room temperature. Immunoreactions were visualized with 3,3′-diaminobenzidine (DAB), and nuclei were stained with Hematoxylin. Sections were photographed with microscope slide scanner Pannoramic MIDI (3D HISTECH).

Immunofluorescence

For immunofluorescence staining, the sections were deparaffinized, rehydrated, antigen repair with EDTA antigen retrieval solution (pH 9.0), washed in PBS briefly and blocked with 3% BSA for 1 h at room temperature. Primary antibodies rabbit anti-SOX7 (Sigma–Aldrich, HPA009065, RRID: AB_1857390), rat anti-VE-cadherin (Abcam, ab91064, RRID: AB_2049374) were incubated at 4°C overnight. Then the sections were stained with fluorescent secondary antibodies, Cy3-conjugated donkey anti-rabbit IgG (Jackson, 711-165-152, RRID: AB_2307443) and FITC-conjugated donkey anti-rat IgG (ServiceBio, GB22302) for 1 h at room temperature, and nuclei were stained with 4',6-diamidino-2-phenylindole (DAPI). Image acquisition was conducted using Nikon microscope.

Collagen gel assay

Explants from E10.5 proximal OFT were cultured following standard protocols as described [26]. In brief, collagen gel was prepared with 10× Medium 199 (Gibco, 11825015) and rat tail type I collagen (Corning, 354236), and neutralized with (10×) 2.2% $NaHCO_3$. The final collagen solution was allowed to polymerize for 2 h at 37°C. Next, the gels were incubated overnight with 1× DMEM supplemented with 10% FBS, 1% insulin-transferrin-selenium-X (ITS-X,

Gibco, 5150056), 100 U/ml penicillin (Gibco, 15140122), and 100 U/ml streptomycin (Gibco, 15140122). The embryonic OFTs were dissected from E10.5 embryos and cultured with the OFT endocardium facing downwards the collagen gel. After attachment, adenovirus infection was used to analyze gain or loss effects of SOX7 on the OFT explants as previously described [27]. To express SOX7, the OFT explants were infected with GFP-tagged adenovirus containing SOX7 (AdV-SOX7) or control adenoviral vectors with no insert (AdV-GFP). To knock down Sox7, OFT explants were infected with GFP-labeled adenovirus encoding siRNA control (AdV-Si-Con, sequence in Supplementary Table S1) or siRNA Sox7 (AdV-Si-Sox7, sequence in Supplementary Table S1). The explants were further cultured for 72 h before the assessment of EndMT. Bright-field images and GFP fluorescent images of OFT explants were taken using Olympus microscope. Explants were fixed and stained with α-smooth muscle actin (α-SMA; Sigma–Aldrich, A5228, RRID: AB_262054) and Alexa Fluor 555-conjugated donkey anti-mouse IgG (Beyotime, A0460) to detect mesenchymal cells. DAPI was used for nuclei staining. The photographs were taken by Leica confocal microscope. Mesenchymal cell migration into the collagen gel was measured and quantified with confocal z-stack images using Image-Pro Plus software. Some explants were immunolabeled for rabbit anti-SOX7 (Sigma–Aldrich, HPA009065, RRID: AB_1857390) and Cy3-conjugated donkey anti-rabbit IgG (Jackson, 711-165-152, RRID: AB_2307443) to verify Sox7 knockdown. ECs were isolated from some OFT explants infected with AdV-GFP or AdV-SOX7 for quantitative real-time polymerase chain reaction (qRT-PCR) analysis. ECs from OFT explants were isolated using collagenase type II (Sigma–Aldrich) by removing the myocardial tissue [28]. ECs from two or three OFT explants were pooled for RNA extraction. RNA was purified using the RNeasy Micro Kit (Qiagen, U.S.A.) following the manufacturer's protocol.

qRT-PCR analysis

Total RNA from each sample was reverse transcribed into complementary DNA by using PrimeScript RT Master Mix (Takara Biotechnology Co., Ltd, Dalian, China). Real-time PCR amplifications were performed on an ABI QuantStudio 3 thermocycler in 20 μl reaction volumes containing cDNA, primers (Supplementary Table S1), and SYBR Green Real-time PCR Master Mix (Takara Biotechnology Co. Ltd, Dalian, China). Thermocycling was performed as follows: initial denaturation at 95°C for 30 s; 45 cycles of denaturation at 95°C for 5 s, and elongation at 60°C for 34 s. The specificity of the PCR was assessed with the melting curves. The $\Delta\Delta C_t$ calculation method was used to quantify the relative gene expression compared with GAPDH or β-actin. All primers were synthesized and purified by Shanghai Sangon Biotechnology Co. Ltd. (Shanghai, China).

Cell proliferation and viability assay

Cell proliferation and viability of HUVECs were measured by the Cell Counting Kit-8 (CCK-8, Yeasen Biotechnology Co., Ltd., Shanghai, China) and 3-(4,5-dimethylthiazol-2-yl)-2,5-diphenyltetrazolium bromide (MTT) Cell Proliferation Kit (Shanghai Sangon Biotechnology Co. Ltd., Shanghai, China) according to the manufacturer's protocol. In brief, HUVECs were seeded into 96-well plates at a density of 1×10^4 cells per well. After being infected with adenovirus-encoding GFP (AdV-GFP) or SOX7 (AdV-SOX7) for 24 and 48 h, cells were detected by CCK-8 and MTT assays. For CCK-8 assay, the cells were incubated with medium containing 10 μl CCK-8 reagents for 1 h at 37°C. The absorbance of the medium was measured at 450 nm using a microplate spectrophotometer (BioTek, Instruments, Inc., Winooski, VT, U.S.A.). For MTT assay, 10 μl MTT solution (5 mg/ml) was added to each well. Following 4-h incubation at 37°C, the cell culture medium was removed, and 100 μl of dimethyl sulfoxide (DMSO) was added and agitated on a shaker for 10 min to fully dissolve the formazan crystals. The absorbance of each well was measured at 570 nm by a microplate spectrophotometer (BioTek, Instruments, Inc., Winooski, VT, U.S.A.).

Wound healing and transwell migration assay

HUVECs were seeded in the six-well plate and cultured in the growth medium in a 37°C incubator. When the cells reached 50–60% confluence, they were infected with adenovirus-encoding GFP (AdV-GFP) or SOX7 (AdV-SOX7). For interference assay, *VE-cadherin* siRNA (Si-VE-cad) or control siRNA (Si-Con) were transfected into cells after 6 h virus infection. In wounding assay, wounds were made with 200 μl sterile pipette tip and washed with PBS to remove the detached cells. Then cells were cultured with fresh medium and images of the wounded region were acquired at 0 and 24 h using an inverted Leica microscope. Movements of cells were calculated using ImageJ software. The changes of scratch area were calculated with initial wound area subtracted from that of 24 h and then divided by the initial one. In transwell assay, 3×10^4 transfected cells suspended in 200 μl serum-free medium seeded in the upper chamber with 8-μm pores (Corning, 3422), 600 μl DMEM with 10% FBS was added to the bottom chamber, incubated in 37°C, 5% CO_2 incubator for 24 h. Cells were fixed with 4% PFA for 30 min at room temperature, washed with PBS, and

Clinical Science (2021) **135** 829–846
https://doi.org/10.1042/CS20201496

stained with Crystal Violet for 20 min. Cells on the inner side of the supports membrane were wiped by cotton swabs, and migrated cells on the outer side were detected using Olymbus microscope. The number of cells in the membrane counted from six randomly selected visual fields (100 magnification) of each filter was averaged.

Electrophoretic mobility shift assay

Electrophoretic mobility shift assay (EMSA) was performed as described previously [29]. Plasmids pcDNA3.1-SOX7 and mutant plasmids were used for the *in vitro* protein synthesis with the TNT®T7 Quick Coupled Transcription/Translation system (Promega, Madison, Wisconsin, U.S.A.) according to the manufacturer's instructions. The oligonucleotides probes (−152/−110 bp) acquired from *VE-cadherin* promoter were synthesized and labeled with biotin in the 5′-end (VE-cadherin biotin, Supplementary Table S1). Unlabeled oligonucleotides with sequences were used as competitors (VE-cadherin comp, Supplementary Table S1). The EMSA was performed using the LightShift Chemiluminescent EMSA kit (LightShift® Chemiluminescent EMSA Kit, Thermo Scientific, U.S.A.) according to the manufacturer's protocol. Briefly, for the binding reactions with volume 20 μl, 5 μl TNT protein product was mixed with 300 fmol of 5′-labeled biotin probes in the following buffer: 2 μl of 10× binding buffer, 2 μl of 50% glycerol, 40 mM KCl, 1 mM EDTA, 0.25 μg poly-deoxyguanylic-deoxycytidylic acid (dGdC). For competitor lanes, a 200-fold excess of competitor DNA was added. Binding reactions were incubated at room temperature for 10 min before the addition of biotin-labeled probe, after which they were incubated for an additional 20 min. The products were then separated by 6% nondenaturing polyacrylamide gels in 0.5× TBE. The DNA–protein complex was electrotransferred to a positively charged nylon membrane, and the signal was detected by the chemiluminescent nucleic acid detection.

Statistical analysis

Data were analyzed by PRISM 6.0 (GraphPad Software Inc., La Jolla, CA, U.S.A.) software and were presented as the mean ± standard error of the mean (S.E.M.). The experiments were repeated at least three times independently. Two-tailed unpaired *t* test was used to determine significant differences between two groups, one-way ANOVA with Tukey's post hoc test or Dunnett's *post hoc* test was used to analyze differences among three or more groups. $P<0.05$ was considered statistically significant.

Results

SOX7 is expressed in the OFT endocardial and mesenchymal cells of the embryonic mouse and human heart

EndMT in OFT is a complex process that initiates at around E10.5 in mice, and at about 30 days (Carnegie stage 13, CS13) in the human fetus. We performed immunohistochemistry analyses for SOX7 in normal mouse and human embryos. At mouse E10.5-E12.5, SOX7 was restricted to the endocardial endothelial and mesenchymal cells in the OFT (Figure 1A, Supplementary Figure S1A), and at human CS13, SOX7 was spatially restricted to the OFT endocardium and mesenchyme (Figure 1B, Supplementary Figure S1B). The endocardial endothelial cells formed the endocardial cushion during EndMT [30], implicating SOX7 in this particular process.

SOX7 is a negative regulator of EndMT in OFT explant cultures

In vitro collagen gel assays were performed to investigate the potential roles of SOX7 in EndMT during OFT development. Proximal OFT explants were dissected from WT embryos at E10.5 and cultured on a collagen matrix for gain and loss function analyses. OFT explants were infected with green fluorescent protein (GFP)-tagged adenovirus containing SOX7 (AdV-SOX7), or control adenoviral vectors with no insert (AdV-GFP). SOX7 overexpression was verified by real-time polymerase chain reaction (RT-PCR) and immunoblots (Supplementary Figure S2). The AdV-SOX7-infected OFT explants exhibited a significantly reduced migration compared with the controls (Figure 2A). We also observed elongated, spindle-like mesenchymal cells, positive for α-SMA, that migrated through the collagen gel in the control OFT explants. In contrast, the SOX7 overexpression explants transformed very poorly, and rounded cells were readily observed (Figure 2B, left panel). The mesenchymal cells that migrated from the explant into the matrix were quantified. Compared with the controls, mesenchymal cells that colonized the matrix, in AdV-SOX7-infected OFT explants, decreased in number by nearly half (Figure 2B, right panel). By qRT-PCR analysis, the expression of SM22α, FSP1 (mesenchymal markers) and CD44 (a mesenchymal stem cell marker) were all significantly decreased in ECs isolated from OFT explants infected with AdV-SOX7 as compared to control samples, whereas vimentin (a Mesenchymal marker) and Notch3 (EndMT transcriptional factor) were unaffected (Supplementary Figure S3). The above results suggest that SOX7 could be a negative regulator of EndMT in OFT explant cultures.

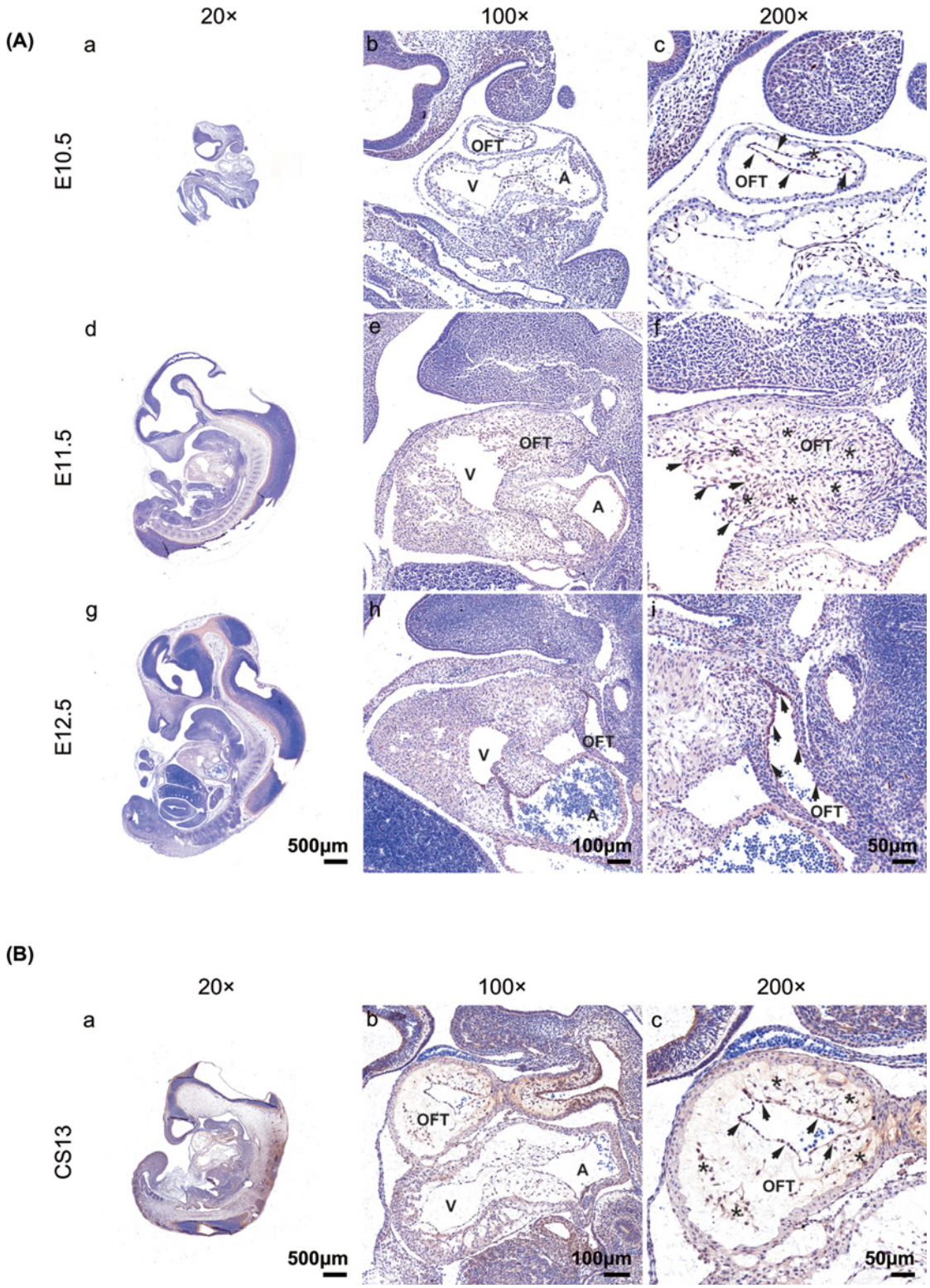

Figure 1. Immunohistochemical staining for SOX7 in OFT during embryonic heart development

(**A**) Distribution of the endogenous Sox7 protein during OFT development at mouse E10.5 (a–c), E11.5 (d–f) and E12.5 (g–i). Strong nuclear staining for Sox7 is seen in the ECs and mesenchymal cells of OFT. (**B**) Distribution of the endogenous SOX7 protein in OFT at human Carnegie Stage 13 (CS13). SOX7 expression in the OFT is limited to the ECs and mesenchymal cells. Representative sagittal sections are shown (n=3 embryos for each stage). Arrowheads, ECs; asterisks, mesenchymal cells. A, atrium; V, ventricle. Scale bars = 500 μm A (a,d,g) and B (a); Scale bars = 100 μm A (b,e,h) and B (b); Scale bars = 50 μm A (c,f,i) and B (c).

Clinical Science (2021) **135** 829–846
https://doi.org/10.1042/CS20201496

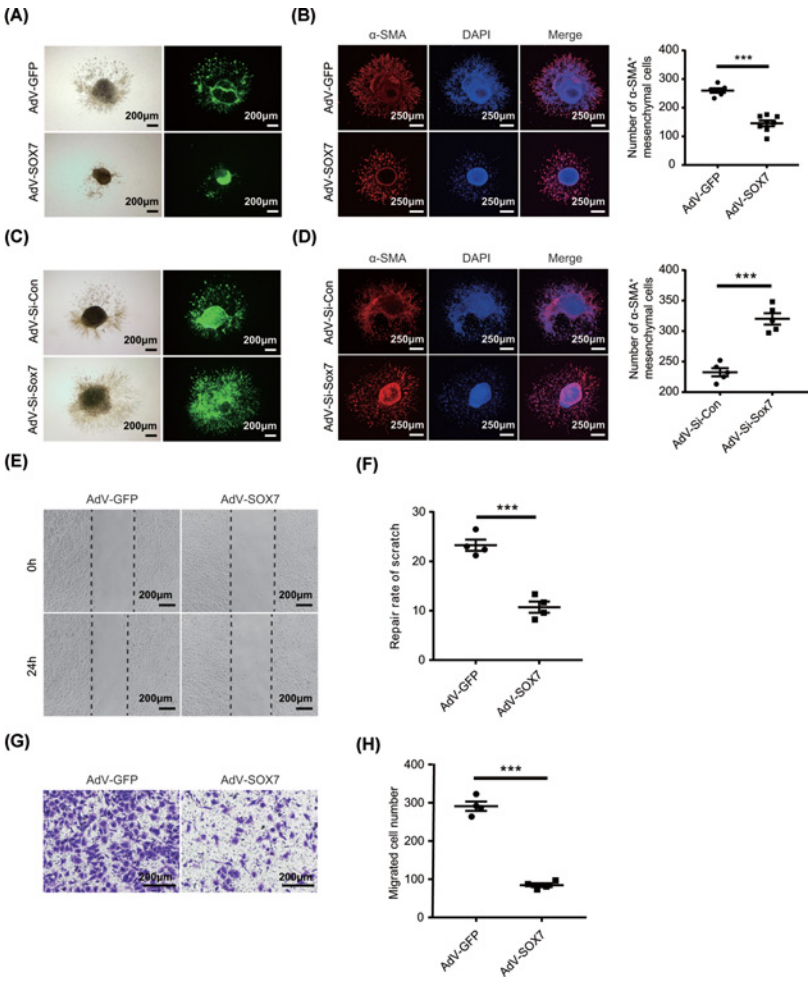

Figure 2. SOX7 inhibits the migration and transition ability of endothelial cells

(**A**,**B**) Gain of SOX7 inhibits EndMT effect. Photomicrographs of OFT explants infected with adenovirus encoding GFP (AdV-GFP) or SOX7 (AdV-SOX7). (A) Left panels are bright field images and right panels are GFP fluorescent images of the same explant. All infected cells are marked by GFP expression (green). Scale bars = 200 μm. (B) Overexpression of SOX7 inhibits the migration of endothelial cells and reduces the amount of mesenchymal cells. (*Left*) Confocal stack of images presented as a maximal projection in the z-axis. α-SMA antibody marks the migrated mesenchymal cells from endothelial cells specificity (red), the nuclei are stained with DAPI (blue), scale bars = 250 μm. (*Right*) Quantitative analysis indicated that the number of migrated mesenchymal cells was significantly reduced in AdV-SOX7 infected explants (n=8) compared with AdV-GFP (n=6). Data shown are the mean ± SEM, two-tailed unpaired t test was used for statistical calculation, ***P<0.001 vs AdV-GFP. (**C**,**D**) Loss of Sox7 promotes EndMT effect. Photomicrographs of OFT explants infected with GFP-labeled adenovirus encoding siRNA control (AdV-Si-Con) or siRNA Sox7 (AdV-Si-Sox7). (C) Left panels are bright field images and right panels are GFP fluorescent images of the same explant. All infected cells are marked by GFP expression (green). Scale bars = 200 μm. (**D**) Knockdown of Sox7 promotes the migration of endothelial cells and increases the amount of mesenchymal cells. (*Left*) Confocal stack of images presented as a maximal projection in the z axes. α-SMA antibody marks the migrated mesenchymal cells from endothelial cells specificity (red), the nuclei are stained with DAPI (blue), scale bars = 250 μm. (*Right*) Quantitative analysis indicated that the number of migrated mesenchymal cells was significantly increased in AdV-Si-Sox7 infected explants (n=5) compared with AdV-Si-Con (n=5). Data shown are the mean ± SEM, two-tailed unpaired t test was used for statistical calculation, ***P<0.001 vs AdV-Si-Con. (**E**–**H**) SOX7 suppresses the migratory ability in endothelial cell line HUVEC. (E,F) Cell wound healing assay for HUVECs migration. (E) Exemplary microphotographs of wound closure in AdV-GFP and AdV-SOX7 groups at 0 and 24 h. Scale bars = 200 μm. (F) Quantitative analysis of the repair rate of scratch. Data are shown as the mean ± SEM, two-tailed unpaired t test was used for statistical calculation, n=4 independent experiments, ***P<0.001 vs AdV-GFP. (G,H) Transwell assay for HUVECs migration. (G) Representative microphotographs of transwell migration detected in HUVECs infected with equal doses of AdV-SOX7 and AdV-GFP adenovirus. Scale bars = 200 μm. (H) Cell migration ability were analyzed by counting cells per field. Data are shown as the mean ± SEM, two-tailed unpaired t test was used for statistical calculation, n=4 independent experiments, ***P<0.001 vs AdV-GFP.

The effect of the knockdown *Sox7* on EndMT were also studied, and knockdown by AdV-Si-Sox7 was verified in immunofluorescence assays (Supplementary Figure S4). The loss of *Sox7* led to a significant increase in mesenchymal cell migration (Figure 2C). Compared with the controls, the AdV-Si-Sox7-infected OFT explants exhibited a scattered and widespread appearance of outgrowing endothelial cells (Figure 2D, left panel). We also counted the number of α-SMA positive mesenchymal cells of outgrowth in each OFT sample, and observed a substantial increase in mesenchymal cells in the *Sox7* knockdown samples compared to the controls (Figure 2D, right panel).

To investigate the effects of SOX7 on endothelial cell phenotype, endothelial cells were infected with AdV-GFP or AdV-SOX7. We firstly performed CCK-8 and MTT assays for cell proliferation and viability and did not observe any obvious difference between the AdV-GFP and AdV-SOX7 infected endothelial cells (Supplementary Figure S5). Then *in vitro* wound healing (scratch) assays revealed a decreased migration of SOX7-expressing endothelial cells at the 24 h timepoint following the endothelial monolayer wounding (Figure 2E). Furthermore, the number of migrating SOX7-expressing cells decreased by almost two thirds (Figure 2F). Transwell assays further showed that SOX7-expressing endothelial cells exhibited a significant decrease in directed migration (Figure 2G,H).

SOX7 inhibits endothelial migration by directly binding to VE-cadherin promoter

Considering the findings that SOX7 inhibits OFT EndMT, we studied the effects of SOX7 signaling on the expression of endothelial and mesenchymal markers by quantitative RT-PCR analysis. The expression of mesenchymal markers (α-SMA, VIMENTIN, FN1) and an endothelial marker (PECAM1) were unaffected, but SOX7 treatment for 24 h increased the mRNA levels of the endothelial gene *VE-cadherin* (Figure 3A). The protein levels of VE-cadherin were analyzed after SOX7 transfection for 48 h and showed similar results (Figure 3B). These findings suggest that VE-cadherin plays an important role in inhibiting EndMT stimulated by SOX7. The distribution of both proteins were analyzed with immunofluorescence staining, which demonstrated that both SOX7 and VE-cadherin are expressed in ECs of the E10.5 OFT (Figure 3C), indicating that there may be some interaction between the two involved in EndMT.

VE-cadherin is the predominant adhesion molecule of the endothelial adherens junction, which decreases in the OFT as EndMT proceeds [31]. To determine whether SOX7 inhibited migration through VE-cadherin, we used a small interfering RNA (siRNA) directed against *VE-cadherin* to reduce protein expression. As shown in Supplementary Figure S6, *VE-cadherin* siRNA successfully knocked down endogenous VE-cadherin expression. The *VE-cadherin* siRNA was transfected into endothelial cells with or without adenovirus-SOX7 transfection. SOX7 suppressed the migration of cells transfected with the control siRNA, but migration suppression was partially reversed by the *VE-cadherin* siRNA in cell wound healing assays (Figure 4A,B). Transwell migration assays yielded similar results, indicating that a reduction in VE-cadherin can compensate for an increase in SOX7 (Figure 4C,D).

To determine if *VE-cadherin* is a downstream *SOX7* effector, we examined whether it is transcriptionally regulated by SOX7. We cloned a ∼580-bp promoter fragment (−534/+45) upstream of VE-cadherin and generated a luciferase reporter, which was co-transfected with a SOX7 expression plasmid into 293T cells. This induced a strong increase in luciferase activity compared with the control (Figure 4E). Similar results were obtained in other cell lines, such as H9C2 (Supplementary Figure S7A) and C2C12 (Supplementary Figure S7B).

We searched for conserved SOX binding sites in *VE-cadherin* promoter sequences using bioinformatics analysis (JASPAR), which predicted two conserved SOX binding sites (Figure 4F). To test whether SOX7 directly binds to the *VE-cadherin* promoter, EMSA was performed using SOX7 protein with a biotin-labeled *VE-cadherin* probe. An *in vitro*-translated SOX7 protein was verified by immunoblot (Supplementary Figure S8). We confirmed the specific binding of SOX7 to the *VE-cadherin* promoter (Figure 4G). The results indicated that the human SOX7 protein was able to directly bind to the *VE-cadherin* promoter sequence. Collectively, these data demonstrate that SOX7 directly binds and transactivates the adhesion protein VE-cadherin. This interaction leads to endothelial cell contact maintenance, migration suppression, and EndMT inhibition during OFT development (Figure 5).

Identification and analysis of candidate SOX7 mutations in OFT defect patients

In an effort to identify *SOX7* sequence changes that contribute to OFT defect development, we screened the coding sequence and intervening intron–exon boundaries of SOX7 in a cohort of 536 patients with CTD (234 TOF, 98 PA/VSD, 13 PA/IVS, 92 TGA, 99 DORV). We identified four nonsynonymous *SOX7* single-nucleotide mutations in four patients with TOF (c.40C>G:p.L14V, c.458G>A:p.R153Q, c.515C>G:p.P172R, c.559G>A:p.G187S), all of which were verified by Sanger sequencing (Figure 6A). The clinical information and *SOX7* mutations in patients

Clinical Science (2021) **135** 829–846
https://doi.org/10.1042/CS20201496

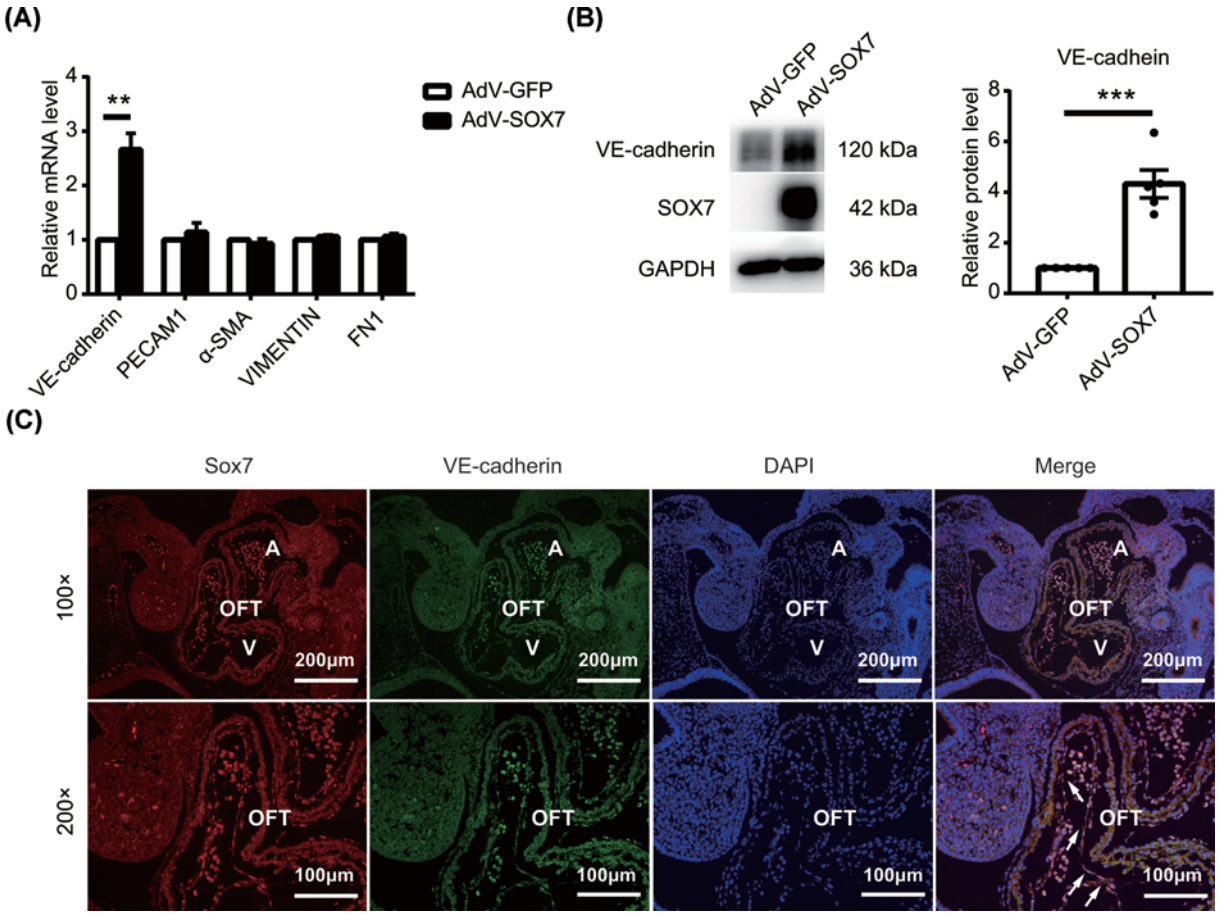

Figure 3. SOX7 induces the endothelial phenotype via up-regulating VE-cadherin

(**A**) Quantitative real-time PCR analysis of the mRNA expression levels of endothelial markers (VE-Cadherin, PECAM-1) and mesenchymal markers (α-SMA, VIMENTIN and FN1) in AdV-GFP and AdV-SOX7 infected HUVECs. Results were normalized to reference gene GAPDH. RNA levels in control (AdV-GFP) are set as 1. Data are shown as the mean ± SEM, two-tailed unpaired *t* test was used for statistical calculation for each marker, $n=3$ independent experiments, $^{**}P<0.01$ vs AdV-GFP. (**B**) (*Left*), Representative immunoblots of VE-cadherin and SOX7 in HUVECs transfected with AdV-GFP and AdV-SOX7. GAPDH was used as internal control. (*Right*), The band density of VE-cadherin on the Western blot of five independent protein samples was digitally quantified by ImageJ software. Data shown are the mean ± SEM, two-tailed unpaired *t* test was used for statistical calculation, $n=5$ per group, $^{***}P<0.001$ vs AdV-GFP. (**C**) Immunofluorescence staining for Sox7 (red) and VE-cadherin (green) in E10.5 embryonic mouse hearts. White arrows denote that both SOX7 and VE-cadherin are expressed in ECs. The experiments were repeated at least three times independently. A, atrium; V, ventricle. Up panel, scale bars = 200 μm; lower panel, scale bars = 100 μm.

with CTD are shown in Table 2. These patients had other CHD, such as atrial septal defect (ASD) and patent foramen ovale (PFO). The identified variant p.L14V, is located before the HMG domain of *SOX7*, whereas the p.R153Q, p.P172R, and p.G187S variants are located between the HMG and transactivation domains, in a region with unknown function (Figure 6B). Homology analysis indicated that three of the variation sites are highly conserved in mammals, except for one mutation, p.G187S, in mice (Figure 6C). None of the variants were found in the 300 controls, but three *SOX7* variants (p.L14V, p.R153Q and p.G187S) were reported in the gnomAD database and p.L14V was reported in the ExAC database (Table 2). Bioinformatics analysis indicated that the p.P172R mutation can cause serious disease based on three pathogenicity prediction programs (mutation taster, SIFT and PolyPhen-2). The other two variants (p.L14V and p.R153Q) were predicted to be disease-causing by two out of the three pathogenicity prediction programs, and the p.G187S mutation was identified as disease-causing in just one pathogenicity prediction program (Table 2).

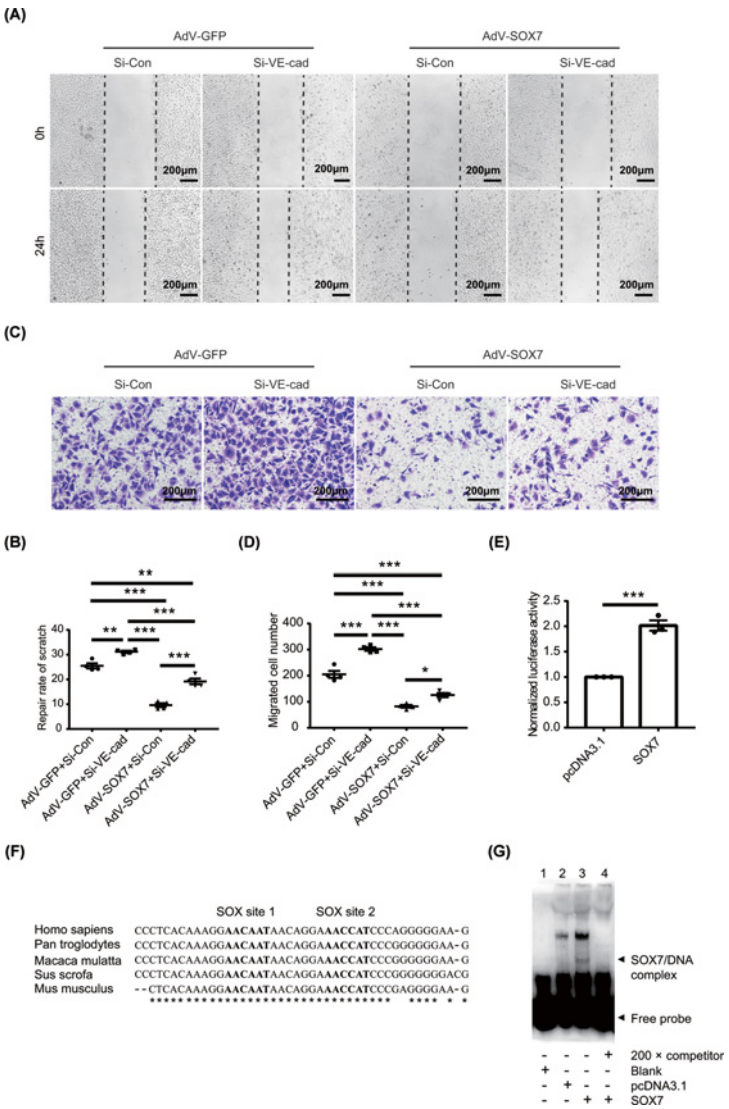

Figure 4. SOX7 inhibited the endothelial migration via directly binding with the *VE-cadherin* promoter

(**A**–**D**) Interference of VE-cadherin impairs the inhibitory effects of SOX7 on endothelial cells migration. HUVECs transfected with *VE-cadherin* siRNA (Si-VE-cad) or with scrambled sequence as a control siRNA (Si-Con) with or without adenovirus-SOX7 transfection. (A,B) Cell wound healing assay for HUVECs migration. (A) Exemplary microphotographs of wound closure at 0 and 24 h. Scale bars = 200 μm. (B) Quantitative analysis of the repair rate of scratch. Data are shown as mean ± SEM, statistical significance was calculated by one-way ANOVA with Tukey's post hoc test, $n=4$ independent experiments, $^{**}P<0.01$, $^{***}P<0.001$. (C,D) Transwell assay for HUVECs migration. (C) Representative microphotographs of transwell migration detected in HUVEC. Scale bars = 200 μm. (D) Cell migration ability was analyzed by counting cells per field. Data are shown as mean ± SEM, statistical significance was calculated by one-way ANOVA with Tukey's post hoc test, $n=4$ independent experiments, $^{*}P<0.05$, $^{***}P<0.001$. (**E**) SOX7 increases the activity of the *VE-cadherin* promoter in 293T cell line. 293T cells were transfected with the *VE-cadherin* promoter luciferase reporter in the presence of control pcDNA3.1 or SOX7 (pcDNA3.1-SOX7) expression vector. The activity of the promoter constructs is expressed relative to that of the control pcDNA3.1. Data are shown as the mean ± SEM, two-tailed unpaired *t* test was used for statistical calculation, $n=3$ independent experiments, $^{***}P<0.001$ vs pcDNA3.1. (**F**) ClustalX analysis showing the DNA sequence used in EMSA of *Homo sapiens* was conserved in *Pan troglodytes*, *Macaca mulatta*, *Sus scrofa* and *Mus musculus*. Two potential SOX binding sites are shown in *boldface*. (**G**) Electrophoretic gel mobility shift assay (EMSA) revealed SOX7 binds with the *VE-cadherin* promoter directly. EMSA was performed using biotin-labeled oligonucleotide probes containing the -152/-110 bp of *VE-cadherin* promoter and in vitro-translated TNT blank protein, TNT pcDNA3.1 protein and TNT SOX7 protein by reticulocyte lysates. A protein–DNA complex was formed (lane 3), which could be inhibited by the addition of 200-fold molar excess unlabeled oligonucleotide probe (lane 4). Arrows indicate: unbind biotin-labeled free probe and SOX7-DNA complex. The experiments were repeated at least three times independently.

Clinical Science (2021) **135** 829–846
https://doi.org/10.1042/CS20201496

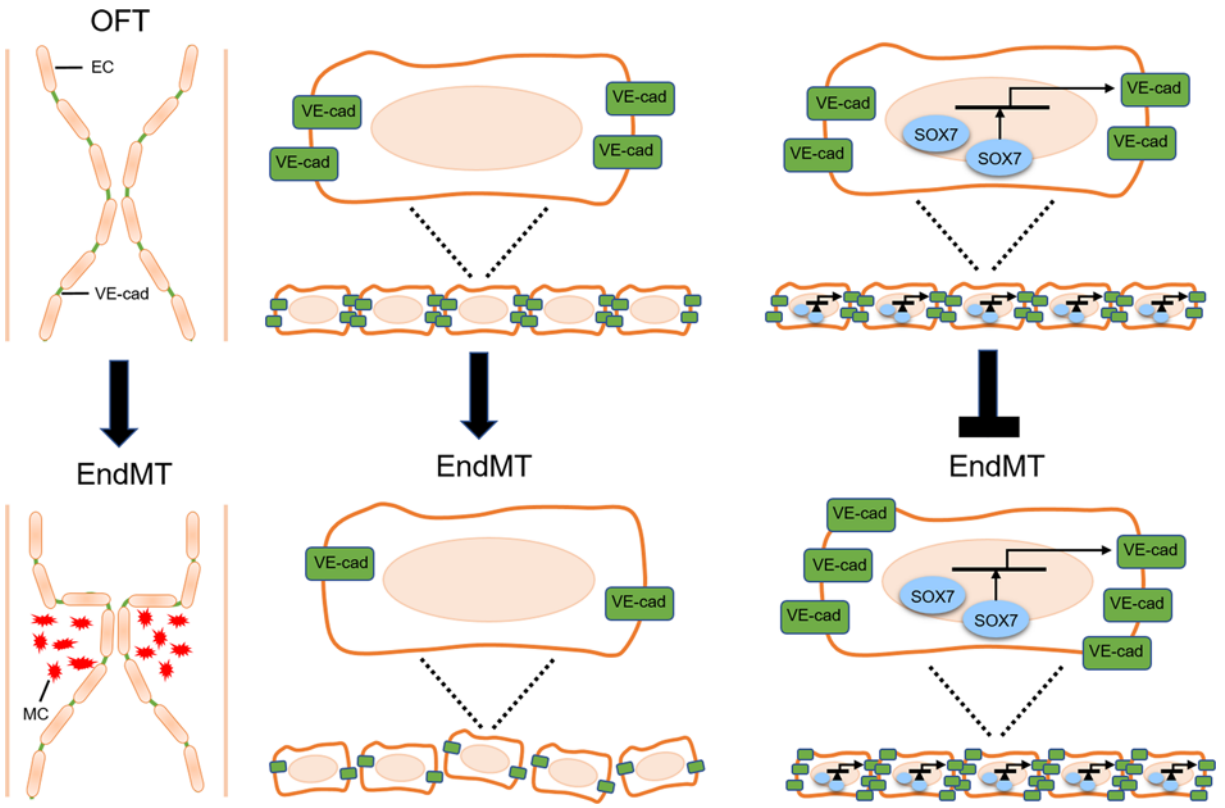

Figure 5. Scheme of the proposed mechanism of SOX7-mediated EndMT suppression during OFT development

SOX7 directly binds and transactivates VE-cadherin in ECs, improving EC contacts and inhibiting EndMT. Abbreviation: MC, mesenchymal cell.

To study the effects of these mutations on SOX7 protein expression, *SOX7* WT and mutant plasmids were transfected into 293T cells. Immunoblotting was used to analyze the expression levels of the WT and mutant SOX7 proteins. Compared with the WT, the normalized gray intensity ratio of the p.P172R protein to GAPDH was significantly reduced. Notably, the expression of the other mutants were not significantly different from the WT (Figure 6D).

WT or mutant SOX7 expression plasmids, with *VE-cadherin* promoter reporter gene vectors, were transfected into 293T, H9C2 and C2C12 cells resperatively to test whether a SOX7 mutation could affect the transcriptional activation of the downstream target VE-cadherin. Compared with the WT, mutants SOX7 p.P172R and p.G187S significantly reduced the transcriptional activation of the *VE-cadherin* promoter in all three cell lines (Figure 6E, Supplementary Figure S9), whereas mutants SOX7 p.L14V and p.R153Q only significantly reduced the transcriptional activation in C2C12 (Supplementary Figure S9B).

EMSA was performed to investigate the DNA-binding capability of the WT and mutant SOX7 proteins. We observed that the mutant SOX7 p.P172R had almost no binding compared to the WT. The p.R153Q and p.G187S mutants showed a slightly weaker binding to the probe, and the p.L14V mutant protein was not significantly different from the WT. Notably, the binding band of the mutant p.R153Q was located higher than the other binding bands (Figure 6F).

Discussion

Although SOX7 has been associated with cardiovascular development, its functional roles during OFT development have not been fully elucidated, which was the goal of this study. SOX7 expression is mainly restricted to the endocardial endothelial and mesenchymal cells of the OFT. The results of the gain and loss function analyses suggested that SOX7 may function as a negative regulator of EndMT by increasing the endothelial marker VE-cadherin during OFT valve morphogenesis. These findings provided a link between SOX7 and VE-cadherin during endocardial development.

SOX7, together with *SOX17* and *SOX18*, belong to the Sox F subgroup that plays significant roles in regulating embryonic development and determining cell fate [24,32]. And SOX7 was previously reported to play an important

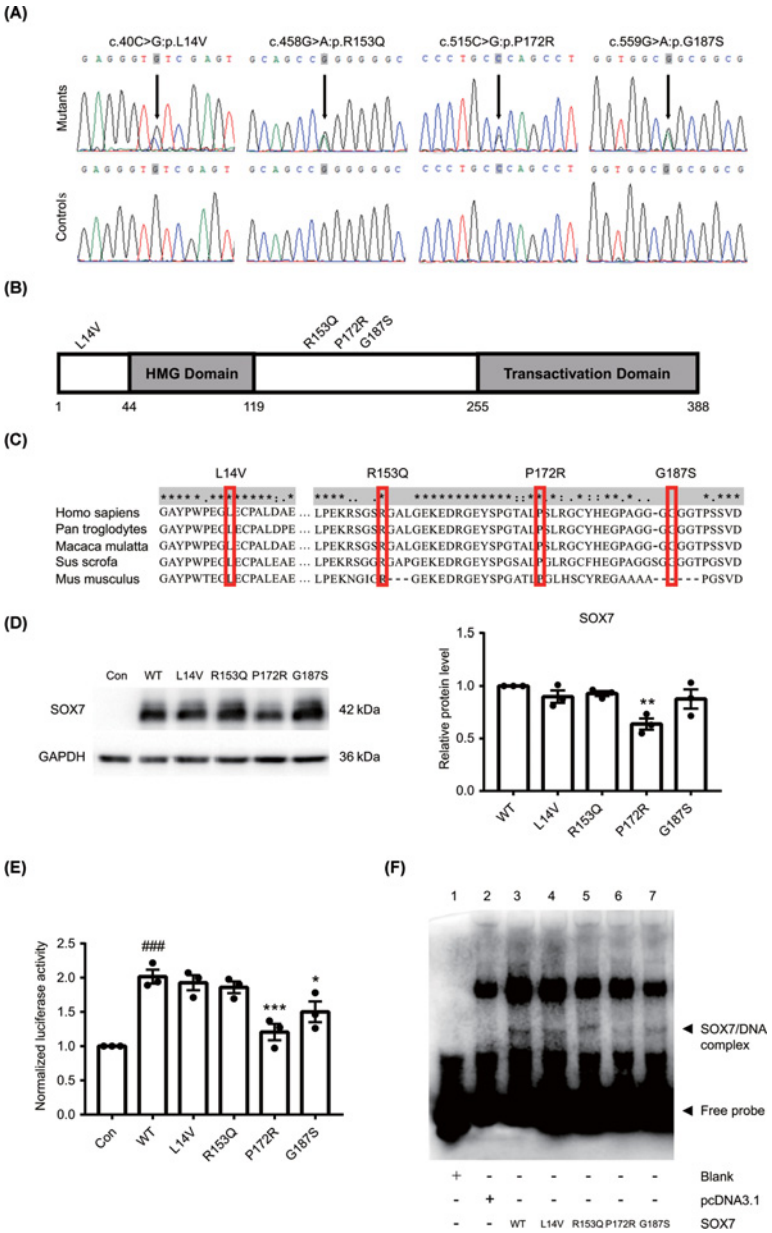

Figure 6. Mutation analysis of SOX7

(**A**) Sanger sequencing validation of *SOX7* mutations. Sequencing chromatograms of four heterozygous missense variants. (**B**) Diagram of *SOX7* protein with location of variants identified in this study. (**C**) ClustalX alignment of the amino acids of the SOX7 mutant proteins among different species. Stars indicate identical residues and dots indicate similar residues. (**D**) Analysis of mutant SOX7 protein expression. Con means transfection of pcDNA3.1 empty vector, WT means transfection of wild-type SOX7 plasmid, L14V, R153Q, P172R, G187S means transfection of different mutant SOX7 plasmids respectively. Use GAPDH as the internal control (left panel). All protein expression was quantitated with ImageJ software. Protein expression levels in mutant samples were normalized to WT protein (right panel). Data are shown as mean ± SEM, statistical significance was calculated by one-way ANOVA with Dunnett's *post hoc* test, $n=3$ independent protein samples, $^{**}P<0.01$ vs WT. (**E**) Effects of SOX7 mutations on transcriptional activation of downstream target gene *VE-cadherin*. Cotransfection of *VE-cadherin* promoter luciferase reporter with the WT and mutant SOX7 protein in 293T cells. The luciferase activities were reported as fold increase relative to the activity of the reporter in the presence of an empty expression plasmid (Con). Data are shown as the mean ± SEM, $n=3$ independent experiments. Statistical significance was calculated by one-way ANOVA with Dunnett's *post hoc* test, $^{*}P<0.05$ vs WT, $^{***}P<0.001$ vs WT. Two-tailed unpaired *t* test was used for statistical calculation, $^{\#\#\#}P<0.001$ WT vs. Con. (**F**) EMSA analysis with wild SOX7 and mutant SOX7 protein. SOX7 EMSA analysis using indicated *VE-cadherin* probes and SOX7 wild and mutant proteins. Bottom arrows indicated unbounded probe, and above arrows indicated shifted complex. The experiments were repeated at least three times independently.

Clinical Science (2021) **135** 829–846
https://doi.org/10.1042/CS20201496

role in vertebrate cardiovascular development [24,33]. Furthermore, SOX7 was also reported to act as a tumor suppressor by inhibiting the migration and invasion of various cancer cells during tumorigenesis, including breast cancer, lung cancer, osteosarcoma, and renal cell carcinoma [34–38]. Endothelial cell migration and invasion into matrix-rich cushions is characteristic of EndMT [5,39], therefore, we explored whether SOX7 is involved in this critical process during OFT development. We demonstrated that SOX7 is specifically expressed in the OFT endocardial and mesenchymal cells, which are the major site of EndMT actions during OFT development. This result indicated that SOX7 may be involved in EndMT. Furthermore, *in vitro* collagen gel assays, paired with *SOX7* knockdown and overexpression studies, confirmed that SOX7 suppresses EndMT during OFT development by inhibiting cell migration, which is similar to the mechanism of SOX7-mediated tumor suppression via migration inhibition [16]. In addition, other SOX family members, such as *Sox17*, *Sox4*, *Sox9*, and *Sox11*, are reportedly essential for the development of the endocardial cushion in the OFT [40–43].

The EndMT program coverts endothelial cells into migratory mesenchymal cells, which is a crucial process during OFT valvulogenesis and septation. Several signaling molecules are involved in EndMT, including the transforming growth factor (TGF)-β [8,44,45], vascular endothelial growth factor [46,47], Notch [48], Snail [45], Slug [48], and BMP signaling [44,47,49–51]. However, the mechanisms underlying EndMT are not fully understood. To elucidate the mechanism of SOX7-induced EndMT inhibition, we examined EndMT-related endothelial and mesenchymal markers. The endothelial marker *VE-cadherin* was significantly increased following SOX7 overexpression for 24 h. VE-cadherin is the predominant adhesion molecule of the endothelial adherens junctions [52], and is transcribed throughout the endocardium of E8.5 WT embryos. Down-regulation of VE-cadherin is considered a key event in EndMT. Furthermore, SOX7 suppressed the migration of endothelial cells by enhancing the expression of the adhesion protein VE-cadherin, and VE-cadherin knockdown partly restored the SOX7-induced suppression of migration. The expression of SOX7 and VE-cadherin are both expressed in ECs of the OFT. Taken together, these results support a model in which SOX7 negatively regulates cell migration in the endocardial cushions, and an increase in SOX7 reinforces cell membrane attachment at focal adhesion sites to reduce the migratory ability of ECs.

Costa et al. reported that SOX7 directly regulates VE-cadherin expression in the mouse hemogenic endothelium at the onset of hematopoietic development [13]; however, there are no reports that examine how SOX7 regulates VE-cadherin during human development or tumorigenesis. We searched for SOX binding sites located in the *VE-cadherin* promoter with bioinformatics analyses, which revealed two highly conserved SOX binding sites. The EMSA results indicated that SOX7 functions as a strong transcriptional activator of VE-cadherin by directly binding to the 5′-(A/T)(A/T)CAA(A/T)G-3′ motif of the gene's promoter. Another group reported that BMP7 blocks TGF-β-induced EndMT by regulating the promoter activity of VE-cadherin [53]. To our knowledge, this is the first evidence that human SOX7 can directly bind to the *VE-cadherin* promoter. Deficiency in VE-cadherin results in abnormal cardiac OFT development. This abnormality manifests as scattered ECs in the center of the OFT at E8.75, and with cell death beyond E9.5 [54]. The levels of VE-cadherin are highly associated with EndMT, and OFT formation requires EndMT. Therefore, an impaired regulation of VE-cadherin may lead to inaccurate septation and valve formation and OFT malformations.

Copy number variations in the *SOX7* gene have been reported in human OFT defects. Previous work in our lab identified three OFT defects (TOF, SV, and DORV/ASD/VSD/PS) in individuals with SOX7 duplication, which was the first published evidence to establish a close relationship between *SOX7* duplication and CTD in clinical specimens [9]. In addition, the overexpression of SOX7 was found to hamper the differentiation of cells and organs, and an up-regulation of SOX7 can cause serious neonatal defects [9]. *SOX7* is also one of the most likely candidate genes associated with 8p23.1 deletion or duplication [55]. It is possible that the dosage imbalance of *SOX7* is responsible for the variety of CTD and septal heart defects found in subjects with imbalances of 8p23.1 [56].

Second-generation sequencing was used to screen *SOX7* mutations in 536 patients with sporadic CTD, and four possible pathogenic mutations were identified in four patients. Furthermore, functional analyses showed that the pathogenicity of the mutant SOX7 may be attributed to the reduced expression or impaired transcription activation of the downstream target gene *VE-cadherin*, due to an impaired DNA-binding capability. With respect to the SOX7 mutant proteins p.P172R and p.G187S, both mutation sites are changed from a hydrophobic to a hydrophilic amino acid; however, the p.L14V mutant protein did not have a different hydropathy index. Thus, we speculated that the binding capacity may be related to amino acid hydrophilicity. In the SOX7 mutant protein p.R153Q, positively charged amino acid become uncharged, and the position of the binding band may be related to an amino acid charge. Expression of the SOX7 mutants affected the expression of VE-cadherin, which suggests that SOX7 can affect OFT development by regulating endocardial EndMT via VE-cadherin.

Our study has several limitations. First, the fact that the loss of VE-cadherin decreases but does not completely abolish SOX7-induced EndMT suppression, indicates that SOX7 can improve cell-cell contacts by upregulating

VE-cadherin. It may also positively affect several other genes involved in the loss of the endothelial phenotype and the gain of the mesenchymal characteristics. Second, *SOX7* mutations have not been validated in a large number of human CTD samples, which requires further research on the subject. Cumulatively, there is insufficient evidence to demonstrate that the *SOX7* mutations reported in this paper are causal for CTD. Well-designed *in vitro* and *in vivo* functional studies are needed to explore the SOX7-CTD mechanism.

In conclusion, SOX7 is exclusively expressed in a subset of endothelial and mesenchymal cells of the OFT where EndMT occurs. OFT explant assays and cell function analyses indicated that SOX7 maintains the endocardial phenotype by directly binding and transactivating the endothelial-specific adhesion molecule VE-cadherin. *SOX7* mutations impair EndMT by regulating VE-cadherin, which may give rise to cardiac OFT defects. Together, these results support a direct role for SOX7 in EndMT of the OFT. This research deepens our understanding of the mechanisms underlying OFT development and CTD, it also provides a basis for early CHD diagnosis and genetic counseling.

Clinical perspectives

- CTD, also known as OFT defect, which causes significant morbidity and mortality. The etiology of most CTD remains poorly understood. We previously reported the identification of a *SOX7* duplication in a pediatric patient in a family with congenital CTD, which was further verified in sporadic cases of CTD, in 2013. However, the molecular mechanisms underlying SOX7 in OFT development and CTD remains unclear.

- SOX7 is exclusively expressed in the endothelial and mesenchymal cells of the OFT where EndMT occurs. OFT explant assays and cell function analyses indicated that SOX7 inhibits EndMT by directly binding and transactivating the promoter of endothelial-specific adhesion molecule VE-cadherin. *SOX7* mutations impair EndMT by regulating VE-cadherin, which may give rise to cardiac OFT defects.

- Our findings support a direct role for SOX7 in EndMT of the OFT. This research deepens our understanding of the mechanisms underlying OFT development and CTD, it also provides a basis for early CHD diagnosis and genetic counseling.

Data Availability

The related data and materials are available for sharing upon request to Xuechao Jiang, Rang Xu, and Kun Sun.

Competing Interests

The authors declare that there are no competing interests associated with the manuscript.

Funding

This work was supported by the National Natural Science Foundation of China [grant numbers 81701488 (to Xuechao Jiang), 81670210 (to Rang Xu)]; and the National Key R&D Program of China [grant number 2018YFC1002400 (to Kun Sun)]. The funding sources were not involved in study design, data collection, data analyses, interpretation, or writing of this manuscript.

CRediT Author Contribution

Xuechao Jiang: Data curation, Formal analysis, Funding acquisition, Investigation, Methodology, Writing—original draft, Project administration. **Tingting Li:** Data curation, Formal analysis, Investigation, Methodology. **Bojian Li:** Methodology. **Wei Wei:** Methodology. **Fen Li:** Resources. **Sun Chen:** Supervision. **Rang Xu:** Conceptualization, Formal analysis, Supervision, Funding acquisition, Validation, Project administration, Writing—review and editing. **Kun Sun:** Conceptualization, Supervision, Funding acquisition, Validation, Project administration, Writing—review and editing.

Acknowledgements

We thank all the individuals who participated in the present study.

Clinical Science (2021) **135** 829–846
https://doi.org/10.1042/CS20201496

Abbreviations

α-SMA, α-smooth muscle actin; CHD, congenital heart defect; CTD, conotruncal defect; DAPI, 4',6-diamidino-2-phenylindole; DORV, double outlet right ventricle; dpc, days post coitus; EC, endocardial cell; EMSA, electrophoretic mobility shift assay; EndMT, endothelial-to-mesenchymal transition; GAPDH, glyceraldehyde 3-phosphate dehydrogenase; HEK, human embryonic kidney; HRP, horseradish peroxidase; HUVEC, human umbilical vein endothelial cell; MTT, 3-(4,5-dimethylthiazol-2-yl)-2,5-diphenyltetrazolium bromide; OFT, outflow tract; PFA, paraformaldehyde; qRT-PCR, quantitative real-time polymerase chain reaction; siRNA, small interfering RNA; SOX, SRY-related HMG-box; SPF, Specific pathogen-free; TGA, transposition of the great artery; TGF, transforming growth factor; TOF, Tetralogy of Fallot; VE-cadherin, vascular endothelial (VE)-cadherin; WT, wild-type.

References

1 Hoffman, J. (2013) The global burden of congenital heart disease. *Cardiovasc. J. Africa* **24**, 141–145, https://doi.org/10.5830/CVJA-2013-028
2 Jain, R., Rentschler, S. and Epstein, J.A. (2010) Notch and cardiac outflow tract development. *Ann. N.Y. Acad. Sci.* **1188**, 184–190, https://doi.org/10.1111/j.1749-6632.2009.05099.x
3 Neeb, Z., Lajiness, J.D., Bolanis, E. and Conway, S.J. (2013) Cardiac outflow tract anomalies. *Wiley Interdiscip. Rev. Dev. Biol.* **2**, 499–530
4 de Lange, F.J., Moorman, A.F., Anderson, R.H., Manner, J., Soufan, A.T., de Gier-de Vries, C. et al. (2004) Lineage and morphogenetic analysis of the cardiac valves. *Circ. Res.* **95**, 645–654, https://doi.org/10.1161/01.RES.0000141429.13560.cb
5 Wu, B., Wang, Y., Lui, W., Langworthy, M., Tompkins, K.L., Hatzopoulos, A.K. et al. (2011) Nfatc1 coordinates valve endocardial cell lineage development required for heart valve formation. *Circ. Res.* **109**, 183–192, https://doi.org/10.1161/CIRCRESAHA.111.245035
6 Hurle, J.M., Colvee, E. and Blanco, A.M. (1980) Development of mouse semilunar valves. *Anat. Embryol. (Berl.)* **160**, 83–91, https://doi.org/10.1007/BF00315651
7 LeMasters, K.E., Blech-Hermoni, Y., Stillwagon, S.J., Vajda, N.A. and Ladd, A.N. (2012) Loss of muscleblind-like 1 promotes invasive mesenchyme formation in endocardial cushions by stimulating autocrine tgfbeta3. *BMC Dev. Biol.* **12**, 22, https://doi.org/10.1186/1471-213X-12-22
8 Potts, J.D., Dagle, J.M., Walder, J.A., Weeks, D.L. and Runyan, R.B. (1991) Epithelial-mesenchymal transformation of embryonic cardiac endothelial cells is inhibited by a modified antisense oligodeoxynucleotide to transforming growth factor beta 3. *Proc. Natl. Acad. Sci. U.S.A.* **88**, 1516–1520, https://doi.org/10.1073/pnas.88.4.1516
9 Long, F., Wang, X., Fang, S., Xu, Y., Sun, K., Chen, S. et al. (2013) A potential relationship among beta-defensins haplotype, sox7 duplication and cardiac defects. *PLoS ONE* **8**, e72515, https://doi.org/10.1371/journal.pone.0072515
10 Cermenati, S., Moleri, S., Cimbro, S., Corti, P., Del Giacco, L., Amodeo, R. et al. (2008) Sox18 and sox7 play redundant roles in vascular development. *Blood* **111**, 2657–2666, https://doi.org/10.1182/blood-2007-07-100412
11 Wat, J.J. and Wat, M.J. (2014) Sox7 in vascular development: review, insights and potential mechanisms. *Int. J. Dev. Biol.* **58**, 1–8, https://doi.org/10.1387/ijdb.130323mw
12 Kim, I.K., Kim, K., Lee, E., Oh, D.S., Park, C.S., Park, S. et al. (2018) Sox7 promotes high-grade glioma by increasing vegfr2-mediated vascular abnormality. *J. Exp. Med.* **215**, 963–983, https://doi.org/10.1084/jem.20170123
13 Costa, G., Mazan, A., Gandillet, A., Pearson, S., Lacaud, G. and Kouskoff, V. (2012) Sox7 regulates the expression of ve-cadherin in the haemogenic endothelium at the onset of haematopoietic development. *Development* **139**, 1587–1598, https://doi.org/10.1242/dev.071282
14 Gandillet, A., Serrano, A.G., Pearson, S., Lie, A.L.M., Lacaud, G. and Kouskoff, V. (2009) Sox7-sustained expression alters the balance between proliferation and differentiation of hematopoietic progenitors at the onset of blood specification. *Blood* **114**, 4813–4822, https://doi.org/10.1182/blood-2009-06-226290
15 Lilly, A.J., Costa, G., Largeot, A., Fadlullah, M.Z., Lie, A.L.M., Lacaud, G. et al. (2016) Interplay between sox7 and runx1 regulates hemogenic endothelial fate in the yolk sac. *Development* **143**, 4341–4351, https://doi.org/10.1242/dev.140970
16 Zhang, Y., Stovall, D.B., Wan, M., Zhang, Q., Chou, J.W., Li, D. et al. (2018) Sox7 target genes and their contribution to its tumor suppressive function. *Int. J. Mol. Sci.* **19**, 1451, https://doi.org/10.3390/ijms19051451
17 Sun, Q.Y., Ding, L.W., Johnson, K., Zhou, S., Tyner, J.W., Yang, H. et al. (2019) Sox7 regulates mapk/erk-bim mediated apoptosis in cancer cells. *Oncogene* **38**, 6196–6210, https://doi.org/10.1038/s41388-019-0865-8
18 Man, C.H., Fung, T.K., Wan, H., Cher, C.Y., Fan, A., Ng, N. et al. (2015) Suppression of sox7 by DNA methylation and its tumor suppressor function in acute myeloid leukemia. *Blood* **125**, 3928–3936, https://doi.org/10.1182/blood-2014-06-580993
19 Takash, W., Canizares, J., Bonneaud, N., Poulat, F., Mattei, M.G., Jay, P. et al. (2001) Sox7 transcription factor: sequence, chromosomal localisation, expression, transactivation and interference with wnt signalling. *Nucleic Acids Res.* **29**, 4274–4283, https://doi.org/10.1093/nar/29.21.4274
20 Taniguchi, K., Hiraoka, Y., Ogawa, M., Sakai, Y., Kido, S. and Aiso, S. (1999) Isolation and characterization of a mouse sry-related cdna, msox7. *Biochim. Biophys. Acta* **1445**, 225–231, https://doi.org/10.1016/S0167-4781(99)00047-0
21 Zhang, C., Basta, T. and Klymkowsky, M.W. (2005) Sox7 and sox18 are essential for cardiogenesis in xenopus. *Dev. Dyn.* **234**, 878–891, https://doi.org/10.1002/dvdy.20565
22 Herpers, R., van de Kamp, E., Duckers, H.J. and Schulte-Merker, S. (2008) Redundant roles for sox7 and sox18 in arteriovenous specification in zebrafish. *Circ. Res.* **102**, 12–15, https://doi.org/10.1161/CIRCRESAHA.107.166066
23 Pendeville, H., Winandy, M., Manfroid, I., Nivelles, O., Motte, P., Pasque, V. et al. (2008) Zebrafish sox7 and sox18 function together to control arterial-venous identity. *Dev. Biol.* **317**, 405–416, https://doi.org/10.1016/j.ydbio.2008.01.028

24 Wat, M.J., Beck, T.F., Hernandez-Garcia, A., Yu, Z., Veenma, D., Garcia, M. et al. (2012) Mouse model reveals the role of sox7 in the development of congenital diaphragmatic hernia associated with recurrent deletions of 8p23.1. *Hum. Mol. Genet.* **21**, 4115–4125, https://doi.org/10.1093/hmg/dds241
25 Li, T., Liu, C., Xu, Y., Guo, Q., Chen, S., Sun, K. et al. (2016) Identification of candidate genes for congenital heart defects on proximal chromosome 8p. *Sci. Rep.* **6**, 36133, https://doi.org/10.1038/srep36133
26 Chen, D., Zhu, X., Kofler, N., Wang, Y., Zhou, B. and Simons, M. (2019) Frs2alpha-dependent cell fate transition during endocardial cushion morphogenesis. *Dev. Biol.* **458**, 88–97
27 Mizuta, K., Sakabe, M., Hashimoto, A., Ioka, T., Sakai, C., Okumura, K. et al. (2015) Impairment of endothelial-mesenchymal transformation during atrioventricular cushion formation in tmem100 null embryos. *Dev. Dyn.* **244**, 31–42, https://doi.org/10.1002/dvdy.24216
28 Luna-Zurita, L., Prados, B., Grego-Bessa, J., Luxan, G., del Monte, G., Benguria, A. et al. (2010) Integration of a notch-dependent mesenchymal gene program and bmp2-driven cell invasiveness regulates murine cardiac valve formation. *J. Clin. Invest.* **120**, 3493–3507, https://doi.org/10.1172/JCI42666
29 Sacilotto, N., Monteiro, R., Fritzsche, M., Becker, P.W., Sanchez-Del-Campo, L., Liu, K. et al. (2013) Analysis of dll4 regulation reveals a combinatorial role for sox and notch in arterial development. *Proc. Natl. Acad. Sci. U.S.A.* **110**, 11893–11898, https://doi.org/10.1073/pnas.1300805110
30 Eisenberg, L.M. and Markwald, R.R. (1995) Molecular regulation of atrioventricular valvuloseptal morphogenesis. *Circ. Res.* **77**, 1–6, https://doi.org/10.1161/01.RES.77.1.1
31 Timmerman, L.A., Grego-Bessa, J., Raya, A., Bertran, E., Perez-Pomares, J.M., Diez, J. et al. (2004) Notch promotes epithelial-mesenchymal transition during cardiac development and oncogenic transformation. *Genes Dev.* **18**, 99–115, https://doi.org/10.1101/gad.276304
32 Bowles, J., Schepers, G. and Koopman, P. (2000) Phylogeny of the sox family of developmental transcription factors based on sequence and structural indicators. *Dev. Biol.* **227**, 239–255, https://doi.org/10.1006/dbio.2000.9883
33 Sakamoto, Y., Hara, K., Kanai-Azuma, M., Matsui, T., Miura, Y., Tsunekawa, N. et al. (2007) Redundant roles of sox17 and sox18 in early cardiovascular development of mouse embryos. *Biochem. Biophys. Res. Commun.* **360**, 539–544, https://doi.org/10.1016/j.bbrc.2007.06.093
34 Hu, W., Han, Y., Yang, W., Xu, B., Zhang, W., Jin, Z. et al. (2019) Novel role of sex-determining region y-box 7 (sox7) in tumor biology and cardiovascular developmental biology. *Semin. Cancer Biol.* **67**, 49–56, https://doi.org/10.1016/j.semcancer.2019.08.032
35 Stovall, D.B., Wan, M., Miller, L.D., Cao, P., Maglic, D., Zhang, Q. et al. (2013) The regulation of sox7 and its tumor suppressive role in breast cancer. *Am. J. Pathol.* **183**, 1645–1653, https://doi.org/10.1016/j.ajpath.2013.07.025
36 Bao, Y., Chen, B., Wu, Q., Hu, K., Xi, X., Zhu, W. et al. (2017) Overexpression of mir-664 is associated with enhanced osteosarcoma cell migration and invasion ability via targeting sox7. *Clin. Exp. Med.* **17**, 51–58, https://doi.org/10.1007/s10238-015-0398-6
37 Stovall, D.B., Cao, P. and Sui, G. (2014) Sox7: from a developmental regulator to an emerging tumor suppressor. *Histol. Histopathol.* **29**, 439–445
38 Wang, L., Fan, Y., Zhang, L., Li, L., Kuang, G., Luo, C. et al. (2019) Classic sry-box protein sox7 functions as a tumor suppressor regulating wnt signaling and is methylated in renal cell carcinoma. *FASEB J.* **33**, 254–263, https://doi.org/10.1096/fj.201701453RR
39 Mjaatvedt, C.H., Lepera, R.C. and Markwald, R.R. (1987) Myocardial specificity for initiating endothelial-mesenchymal cell transition in embryonic chick heart correlates with a particulate distribution of fibronectin. *Dev. Biol.* **119**, 59–67, https://doi.org/10.1016/0012-1606(87)90206-5
40 Saba, R., Kitajima, K., Rainbow, L., Engert, S., Uemura, M., Ishida, H. et al. (2019) Endocardium differentiation through sox17 expression in endocardium precursor cells regulates heart development in mice. *Sci. Rep.* **9**, 11953, https://doi.org/10.1038/s41598-019-48321-y
41 Schilham, M.W., Oosterwegel, M.A., Moerer, P., Ya, J., de Boer, P.A., van de Wetering, M. et al. (1996) Defects in cardiac outflow tract formation and pro-b-lymphocyte expansion in mice lacking sox-4. *Nature* **380**, 711–714, https://doi.org/10.1038/380711a0
42 Akiyama, H., Chaboissier, M.C., Behringer, R.R., Rowitch, D.H., Schedl, A., Epstein, J.A. et al. (2004) Essential role of sox9 in the pathway that controls formation of cardiac valves and septa. *Proc. Natl. Acad. Sci. U.S.A.* **101**, 6502–6507, https://doi.org/10.1073/pnas.0401711101
43 Sock, E., Rettig, S.D., Enderich, J., Bosl, M.R., Tamm, E.R. and Wegner, M. (2004) Gene targeting reveals a widespread role for the high-mobility-group transcription factor sox11 in tissue remodeling. *Mol. Cell. Biol.* **24**, 6635–6644, https://doi.org/10.1128/MCB.24.15.6635-6644.2004
44 Yamagishi, T., Ando, K. and Nakamura, H. (2009) Roles of tgfbeta and bmp during valvulo-septal endocardial cushion formation. *Anat. Sci. Int.* **84**, 77–87, https://doi.org/10.1007/s12565-009-0027-0
45 Kokudo, T., Suzuki, Y., Yoshimatsu, Y., Yamazaki, T., Watabe, T. and Miyazono, K. (2008) Snail is required for tgfbeta-induced endothelial-mesenchymal transition of embryonic stem cell-derived endothelial cells. *J. Cell Sci.* **121**, 3317–3324, https://doi.org/10.1242/jcs.028282
46 Stankunas, K., Ma, G.K., Kuhnert, F.J., Kuo, C.J. and Chang, C.P. (2010) Vegf signaling has distinct spatiotemporal roles during heart valve development. *Dev. Biol.* **347**, 325–336, https://doi.org/10.1016/j.ydbio.2010.08.030
47 Bai, Y., Wang, J., Morikawa, Y., Bonilla-Claudio, M., Klysik, E. and Martin, J.F. (2013) Bmp signaling represses vegfa to promote outflow tract cushion development. *Development* **140**, 3395–3402, https://doi.org/10.1242/dev.097360
48 Niessen, K., Fu, Y., Chang, L., Hoodless, P.A., McFadden, D. and Karsan, A. (2008) Slug is a direct notch target required for initiation of cardiac cushion cellularization. *J. Cell Biol.* **182**, 315–325, https://doi.org/10.1083/jcb.200710067
49 Liu, W., Selever, J., Wang, D., Lu, M.F., Moses, K.A., Schwartz, R.J. et al. (2004) Bmp4 signaling is required for outflow-tract septation and branchial-arch artery remodeling. *Proc. Natl. Acad. Sci. U.S.A.* **101**, 4489–4494, https://doi.org/10.1073/pnas.0308466101
50 Ma, L., Lu, M.F., Schwartz, R.J. and Martin, J.F. (2005) Bmp2 is essential for cardiac cushion epithelial-mesenchymal transition and myocardial patterning. *Development* **132**, 5601–5611, https://doi.org/10.1242/dev.02156
51 McCulley, D.J., Kang, J.O., Martin, J.F. and Black, B.L. (2008) Bmp4 is required in the anterior heart field and its derivatives for endocardial cushion remodeling, outflow tract septation, and semilunar valve development. *Dev. Dyn.* **237**, 3200–3209, https://doi.org/10.1002/dvdy.21743
52 Lampugnani, M.G., Resnati, M., Raiteri, M., Pigott, R., Pisacane, A., Houen, G. et al. (1992) A novel endothelial-specific membrane protein is a marker of cell-cell contacts. *J. Cell Biol.* **118**, 1511–1522, https://doi.org/10.1083/jcb.118.6.1511

Clinical Science (2021) **135** 829–846
https://doi.org/10.1042/CS20201496

53 Xu, X., Friehs, I., Zhong Hu, T., Melnychenko, I., Tampe, B., Alnour, F. et al. (2015) Endocardial fibroelastosis is caused by aberrant endothelial to mesenchymal transition. *Circ. Res.* **116**, 857–866, https://doi.org/10.1161/CIRCRESAHA.116.305629
54 Carmeliet, P., Lampugnani, M.G., Moons, L., Breviario, F., Compernolle, V., Bono, F. et al. (1999) Targeted deficiency or cytosolic truncation of the ve-cadherin gene in mice impairs vegf-mediated endothelial survival and angiogenesis. *Cell* **98**, 147–157, https://doi.org/10.1016/S0092-8674(00)81010-7
55 Wat, M.J., Shchelochkov, O.A., Holder, A.M., Breman, A.M., Dagli, A., Bacino, C. et al. (2009) Chromosome 8p23.1 deletions as a cause of complex congenital heart defects and diaphragmatic hernia. *Am. J. Med. Genet. A* **149A**, 1661–1677, https://doi.org/10.1002/ajmg.a.32896
56 Barber, J.C., Rosenfeld, J.A., Foulds, N., Laird, S., Bateman, M.S., Thomas, N.S. et al. (2013) 8p23.1 duplication syndrome; common, confirmed, and novel features in six further patients. *Am. J. Med. Genet. A* **161A**, 487–500, https://doi.org/10.1002/ajmg.a.35767

Supplementary material

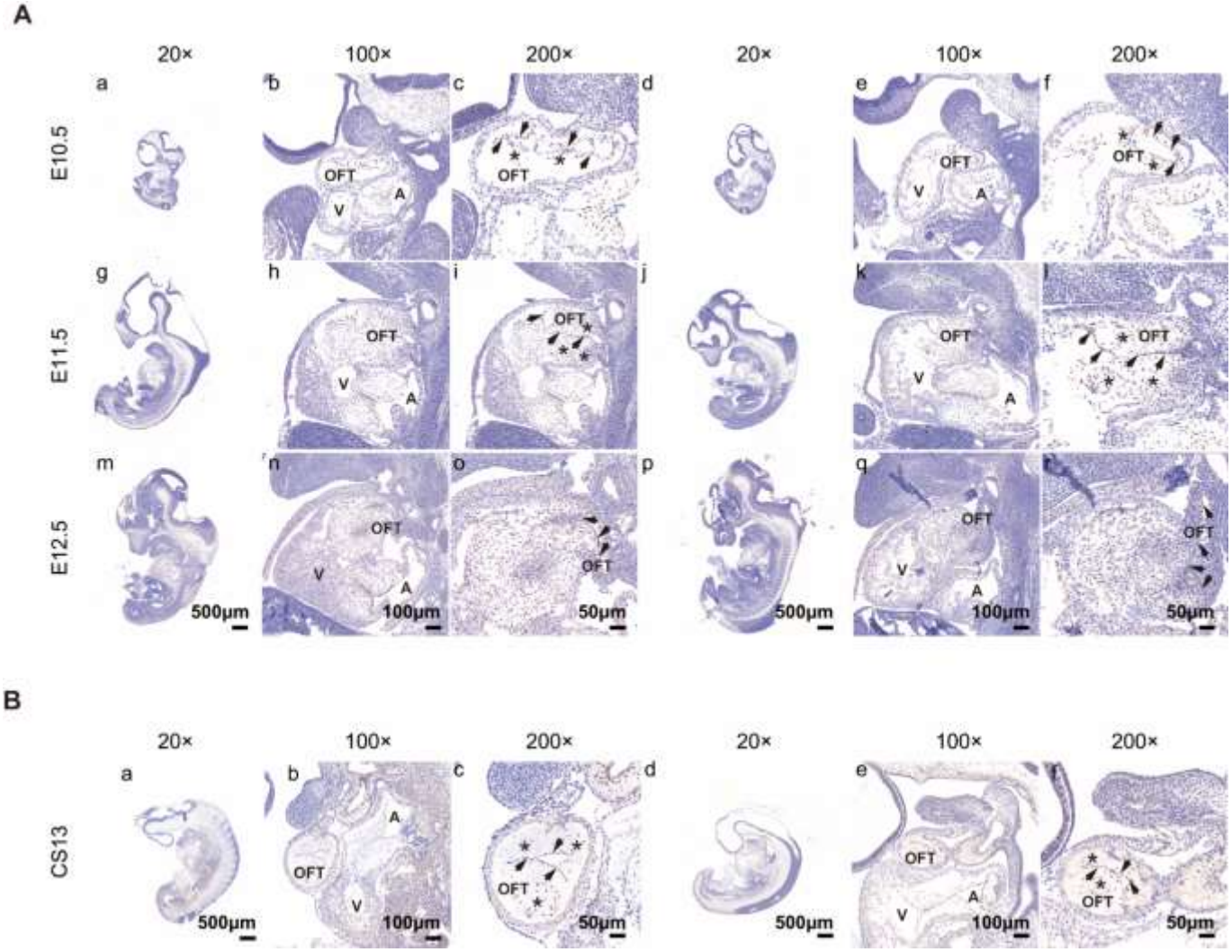

Figure S1. Immunohistochemical staining for SOX7 in OFT during embryonic heart development.

(**A**) Distribution of the endogenous Sox7 protein during OFT development at mouse E10.5 (a-f), E11.5 (g-l) and E12.5 (m-r). Strong nuclear staining for Sox7 is seen in the endocardial cells and mesenchymal cells of OFT. (**B**) Distribution of the endogenous SOX7 protein in OFT at human Carnegie Stage 13 (CS13).SOX7 expression in the OFT is limited to the endocardial cells and mesenchymal cells. Images of the other two embryos at each stageare shown. Arrowheads, endocardial cells; asterisks, mesenchymal cells. OFT, outflow tract; A, atrium; V, ventricle. Scale bars=500 μm A (a, d, g, j, m, p) and B (a, d); Scale bars=100 μm A (b, e, h, k, n, q) and B (b, e); Scale bars=50 μm A (c, f, i, l, o, r) and B (c, f).

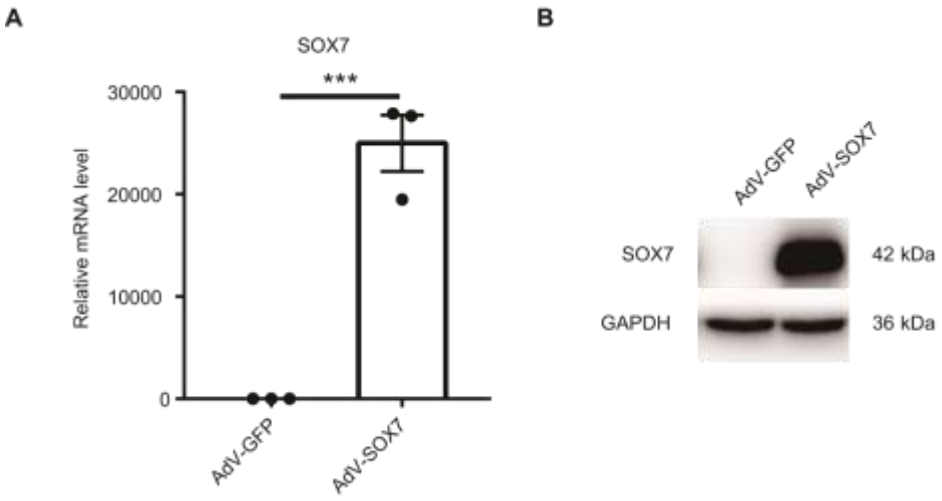

Figure S2. Verification of SOX7 overexpression.

(**A**) Quantitative real-time PCR analysis of the mRNA expression levels of SOX7 in AdV-GFP and AdV-SOX7 infected HUVECs. Results were normalized to reference gene GAPDH. RNA levels in control (AdV-GFP) are set as 1. Data are shown as the mean ± SEM, two-tailed unpaired T test was used for statistical calculation, n=3independent experiments, ***p<0.001 vs AdV-GFP. (**B**) Representative immunoblots of SOX7 in HUVECs transfected with AdV-GFP and AdV-SOX7. GAPDH was used as internal control. Repeat at least 3 independent experiments.

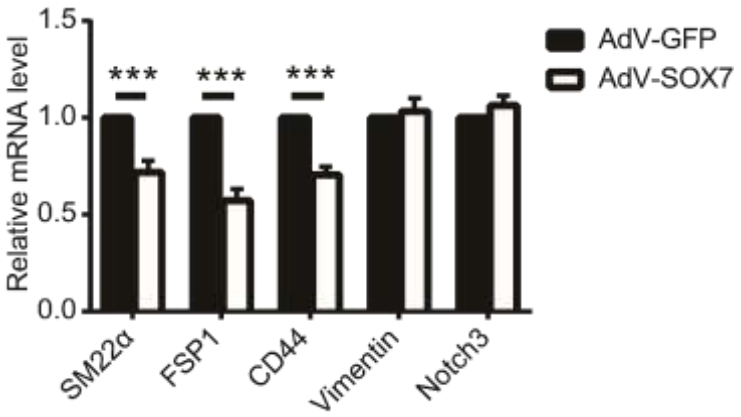

Figure S3.Analysis of EndMT marker expression by qRT-PCR in ECs isolated from OFT explants infected with AdV-GFP or AdV-SOX7.

Quantitative real-time PCR analysis of the mRNA expression levels of mesenchymal markers (SM22α, FSP1 and Vimentin), mesenchymal stem cell marker (CD44) and EndMT transcriptional factor (Notch3) in ECs isolated from OFT explants infected with AdV-GFP or AdV-SOX7. Results were normalized to reference gene β-actin. RNA levels in control (AdV-GFP) are set as 1. Data are shown as the mean ± SEM, two-tailed unpaired T test was used for statistical calculation for each marker, n=7 independent samples per group, ***$p<0.001$ vs AdV-GFP.

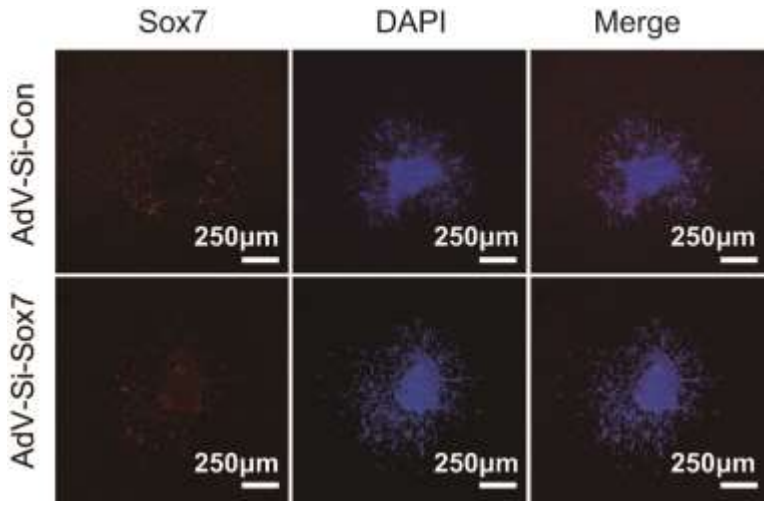

Figure S4. Verification of Sox7 knockdown.

Representative photomicrographs of OFT explants infected with GFP labeled adenovirus encoding siRNA control (AdV-Si-Con) or siRNA Sox7 (AdV-Si-Sox7). Sox7 (red), the nuclei are stained with DAPI (blue), scale bars=250 μm. Repeat 3 independent experiments.

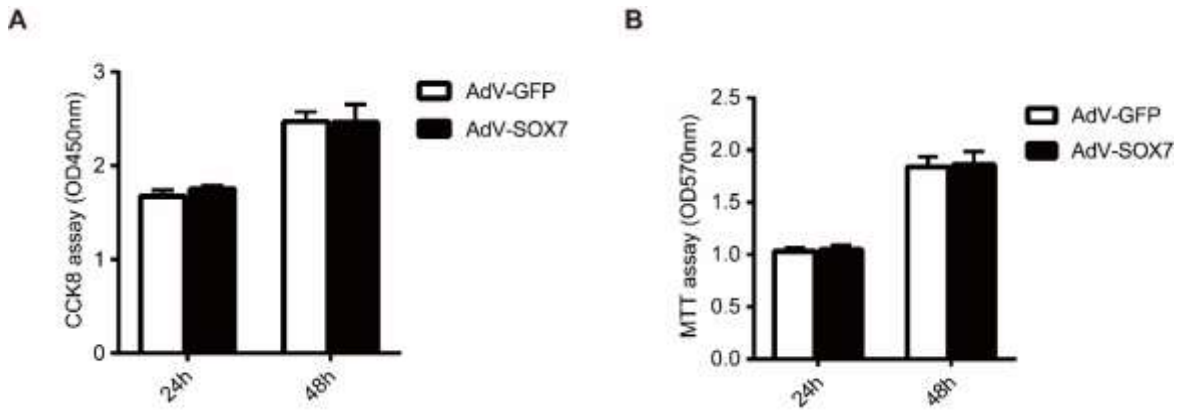

Figure S5. Effects of SOX7 on cell proliferation and viability in HUVECs.

(**A** and **B**) Cell proliferation and viability of HUVEC infected with AdV-Con or AdV-SOX7 for 24 h, 48h by CCK-8 assay and MTT assay. Data are shown as the mean ± SEM, two-tailed unpaired T test was used for statistical calculation for each time point, n= 3 independent experiments, each consisting of 6 different wells. *$p<0.05$ vs AdV-GFP group.

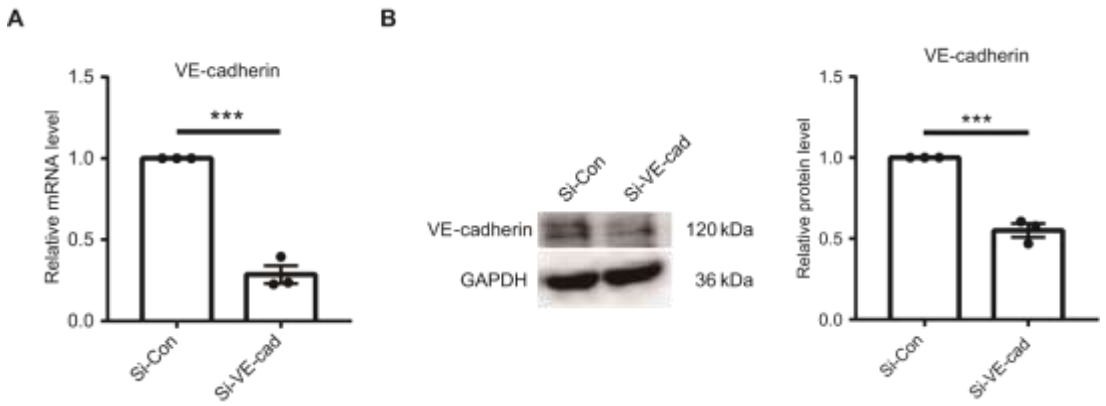

Figure S6. Verification of VE-cadherin knockdown

(**A**) Quantitative real-time PCR analysis of the mRNA expression levels of VE-cadherin in Si-Con and Si-VE-cad transfected HUVECs. Results were normalized to reference gene GAPDH. RNA levels in control (Si-Con) are set as 1. Data are shown as the mean ± SEM, two-tailed unpaired T test was used for statistical calculation, n=3 independent experiments, ***p<0.001 vs Si-Con. (**B**) (*Left*) Representative immunoblots of VE-cadherin in HUVECs transfected with Si-Con and Si-VE-cad. GAPDH was used as internal control. (*Right*), The band density of VE-cadherin on the Western blot of three independent protein samples was digitally quantified by ImageJ software. Data shown are the mean ± SEM, two-tailed unpaired T test was used for statistical calculation, n=3 per group, ***p<0.001 vs Si-Con.

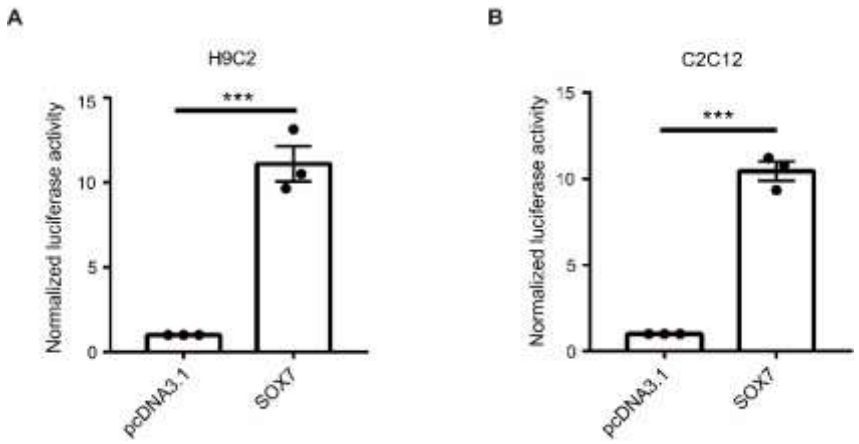

Figure S7. SOX7 increases the activity of the *VE-cadherin* promoter in H9C2 and C2C12 cell lines.

(**A**and**B**) Cells were transfected with the *VE-cadherin* promoter luciferase reporter in the presence of control pcDNA3.1 or SOX7 (pcDNA3.1-SOX7) expression vector. The activity of the promoter constructs is expressed relative to that of the control pcDNA3.1 for each cell line. Data are shown as the mean ± SEM, two-tailed unpaired T test was used for statistical calculation, n=3 independent experimentsfor H9C2 andC2C12, ***$p<0.001$ vs. pcDNA3.1.

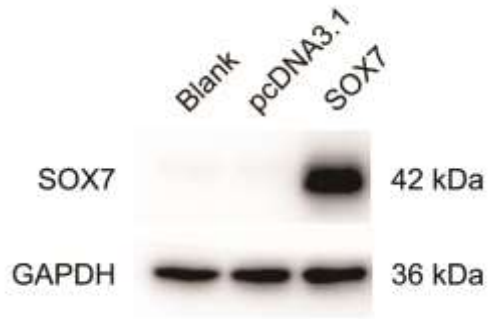

Figure S8. Verification of in vitro-translated SOX7 by reticulocyte lysates.

Representative immunoblots of SOX7 with in vitro-translated TNT blank protein, TNT pcDNA3.1 protein and TNT SOX7 protein. GAPDH was used as internal control. Repeat 3 independent experiments.

.

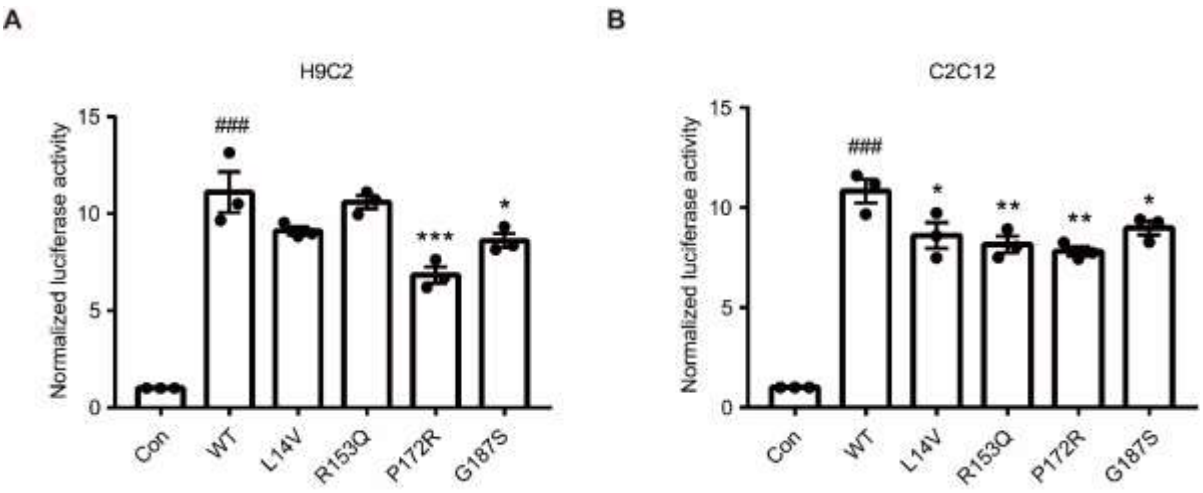

Figure S9. Effects of SOX7 mutations on transcriptional activation of downstream target gene *VE-cadherin*in H9C2 and C2C12 cells. Cotransfection of *VE-cadherin* promoter luciferase reporter with the WT and mutant SOX7 protein in H9C2 (**A**) and C2C12 cells (**B**). The luciferase activities were reported as fold increase relative to the activity of the reporter in the presence of an empty expression plasmid (Con). Data are shown as the mean ± SEM, n=3 independent experiments. Statistical significance was calculated by one-way ANOVA with Dunnett's*post hoc* test, *P<0.05 vs WT, **P<0.01 vs WT, ***P<0.001 vs WT. Two-tailed unpaired T test was used for statistical calculation , ###p<0.001 WT vs. Con.

Table S1 Primers used for PCR, RT-PCR, EMSA and Site-directed mutagenesis

Primer Name	Sequence (5'-3')
PCR (promoter)	
VE-cadhein F	GGGGTACCCCACAAAGACATCATGGGATCACC
VE-cadherin R	CCAAGCTTTTCTGTTCCGTTGGACTGCCT
RT-PCR (human)	
VE-cadherin F	GTTCACGCATCGGTTGTTCAA
VE-cadherin R	CGCTTCCACCACGATCTCATA
PECAM1 F	ACCGTGACGGAATCCTTCTCT
PECAM1 R	GCTGGACTCCACTTTGCAC
α-SMA F	GCTATCCAGGCGGTGCTGTCTCTCT
α-SMA R	GCCAGCCAGATCCAGACGCATGATG
VIMENTIN F	GCAGGTGGACCAGCTAACCAACGA
VIMENTIN R	GCCAGAGACGCATTGTCAACATCCT
FN1 F	CGACGCCTCCACTGCCATTGAT
FN1 R	GCCAGTAATAGTAGCCTCTGTGACACC
SOX7 F	AAGATGCTGGGAAAGTCGTGGAA
SOX7 R	CGCTTGGCCTGCTTCTTCCT
GAPDH F	GAGTCCACTGGCGTCTTCACCACCAT
GAPDH R	GAGGCATTGCTGATGATCTTGAGGCTGTTG
RT-PCR (mouse)	
SM22α F	TGACGAGGAGCTGGAGGAGCGACTA
SM22α R	CAGGCTGTTCACCAATTTGCTCAGAATCAC
FSP1 F	ACTCAGGCAAAGAGGGTGACAAGTTCAAGC
FSP1 R	TGTCCCTGTTGCTGTCCAAGTTGCTCATCA
CD44 F	TCTTGGCATCTCTCCTGGCACTGGCTCTGA
CD44 R	GTCTTCCACCGTCCCATTGCCACCGTTGA
Vimentin F	GTGGATCAGCTCACCAACGACAAGG
Vimentin R	CAGGGTGCTTTCGGCTTCCTCTCT
Notch3 F	TGCTAGAGCGGATGCAGCCAAG
Notch3 R	TGGAGCGGTTCCTGATGAGAATCTG
β-actin F	GGCTGTATTCCCCTCCATCG

β-actin R	CCAGTTGGTAACAATGCCATGT
EMSA	
VE-cadherin biotin F	5’-Biotin-
VE-cadherin biotin R	CCCTCACAAAGGAACAATAACAGGAAACCATCCCAGGGGGAAG
VE-cadherin comp F	5’-Biotin-
VE-cadherin comp R	CTTCCCCCTGGGATGGTTTCCTGTTATTGTTCCTTTGTGAGGG
SiRNA	CCCTCACAAAGGAACAATAACAGGAAACCATCCCAGGGGGAAG
AdV-Si-SOX7 F	CTTCCCCCTGGGATGGTTTCCTGTTATTGTTCCTTTGTGAGGG
AdV-Si-SOX7 R	
Si-VE-cad F	GGATCGCAATGAATTTGATCATGATCAAATTCATTGCGATCC
Si-VE-cad R	GGATCGCAATGAATTTGATCATGATCAAATTCATTGCGATCC
	CCUCUGUCAUGUACCAAAUTT
	AUUUGGUACAUGACAGAGGTT
Site-directed mutagenesis	
c.40C>G:p.L14V F	CCTTGGCCCGAGGGT**G**TCGAGTGCC
c.40C>G:p.L14V R	GGCACTCGA**C**ACCCTCGGGCCAAGG
c.458G>A:p.R153Q F	AAGCGGCAGCC**A**GGGGGCGCTGG
c.458G>A:p.R153Q R	CCAGCGCCCCC**T**GGCTGCCGCTT
c.515C>G:p.P172R F	CACTGCCCTGC**G**CAGCCTCCGGG
c.515C>G:p.P172R R	CCCGGAGGCTG**C**GCAGGGCAGTG
c.559G>A:p.G187S F	CTGGTGGTGGC**A**GCGGCGGCACC
c.559G>A:p.G187S R	GGTGCCGCCGC**T**GCCACCACCAG

F, forward primers; R, reverse primers. Underlines represent restriction sites placed in the primers, GGTACC: *Kpn* Ⅰ , AAGCTT:*Hind Ⅲ*. VE-cadherin comp represents competition probe. Si-VE-cad: SiRNA VE-cadherin. Boldface indicates nucleotide changes in the oligo sequences.